Molecular Cell

Article

H2AK119ub1-MLL2 counteraction underlies heritable H3K27me3 formation in oocytes

Graphical abstract

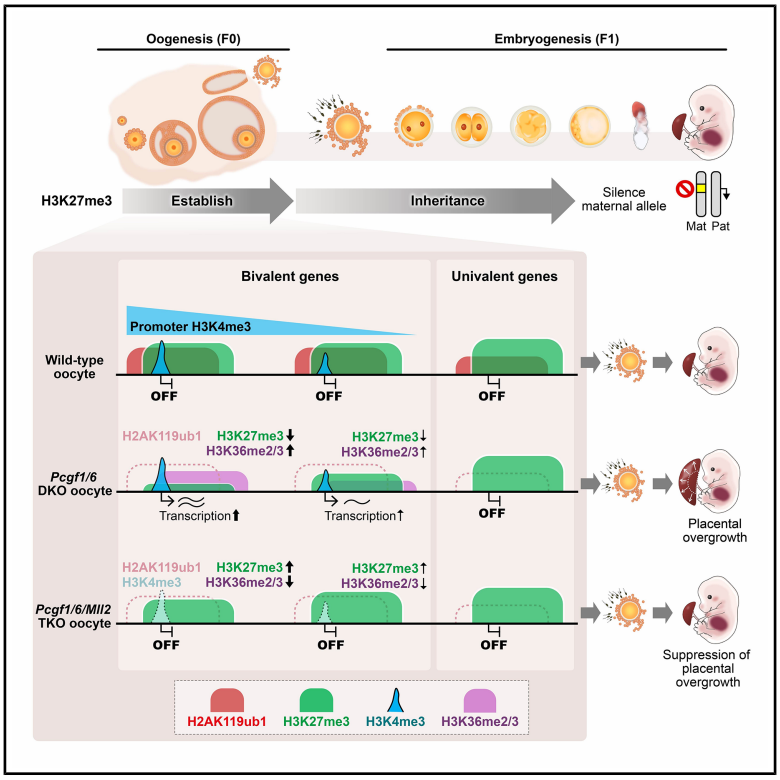

Highlights

- H2AK119ub1 loss reduces H3K27me3 proportionally to basal H3K4me3 levels
- MLL2-H3K4me3 depletion restores H3K27me3 in H2AK119ub1-deficient oocytes
- H3K27me3 restoration also occurs at a key noncanonical imprinted gene, *Sfmbt2*
- The catalytic activity of PRC1 is critical for H3K27me3 deposition in oocytes

Authors

Hailiang Mei, Chisayo Kozuka, Mami Kumon, Haruhiko Koseki, Azusa Inoue

Correspondence

azusa.inoue@riken.jp

In brief

Mei et al. reveal that the Polycomb mark H2AK119ub1 maintains gene silencing in mouse oocytes by opposing MLL2 activity, enabling the establishment of heritable H3K27me3. They uncover how the balance between repressive and activating chromatin mechanisms shapes the maternal epigenome.

Mei et al., 2026, Molecular Cell *86*, 1–17
May 7, 2026
https://doi.org/10.1016/j.molcel.2026.03.014

CellPress

Please cite this article in press as: Mei et al., H2AK119ub1-MLL2 counteraction underlies heritable H3K27me3 formation in oocytes, Molecular Cell (2026), https://doi.org/10.1016/j.molcel.2026.03.014

Molecular Cell

CellPress

Article

H2AK119ub1-MLL2 counteraction underlies heritable H3K27me3 formation in oocytes

Hailiang Mei,[1,5] Chisayo Kozuka,[1] Mami Kumon,[1] Haruhiko Koseki,[3,4] and Azusa Inoue[1,2,5,6,*]
[1]Laboratory for Epigenome Inheritance, RIKEN Center for Integrative Medical Sciences, Yokohama 230-0045, Japan
[2]Tokyo Metropolitan University, Hachioji 192-0397, Japan
[3]Laboratory for Developmental Genetics, RIKEN Center for Integrative Medical Sciences, Yokohama 230-0045, Japan
[4]Department of Cellular and Molecular Medicine, Graduate School of Medicine, Chiba University, Chiba 260-8670, Japan
[5]These authors contributed equally
[6]Lead contact
*Correspondence: azusa.inoue@riken.jp
https://doi.org/10.1016/j.molcel.2026.03.014

SUMMARY

Polycomb group (PcG) and Trithorax group (TrxG) proteins establish bivalent chromatin marked by H3K27me3, H2AK119ub1, and H3K4me3. However, how bivalent chromatin is formed *in vivo* in mammals is poorly understood. In mouse oocytes, it arises at thousands of promoters, including noncanonical imprinted loci whose H3K27me3 is intergenerationally inherited by early embryos. Here, we show that H3K27me3 is deposited at H3K4me3-premarked promoters in an H2AK119ub1-dependent manner during oogenesis. We find that H2AK119ub1 deficiency causes transcriptional derepression and loss of H3K27me3 proportional to preexisting H3K4me3 levels in oocytes. Importantly, concomitant deficiency of H2AK119ub1 and MLL2-mediated H3K4me3 substantially restores transcriptional silencing and H3K27me3 deposition, leading to partial restoration of noncanonical imprinting in offspring. Taken together, we propose that H2AK119ub1 antagonizes MLL2 function to repress bivalent genes during oogenesis, thereby conferring heritable H3K27me3. This study reveals how PcG and TrxG counteraction shapes the maternal epigenome for the next generation's development.

INTRODUCTION

Polycomb group (PcG) and Trithorax group (TrxG) proteins are evolutionarily highly conserved across the metazoan kingdom and play fundamental roles in gene regulation in development and disease.[1–3] PcG and TrxG proteins repress and promote transcription, respectively, and often form long-lasting epigenetic memory. In mammals, PcG includes Polycomb repressive complex 1 (PRC1), PRC2, and their accessory subunits, whereas TrxG includes the MLL and SET1 family proteins. An early genetics study in mice reported that combinatorial mutations of *Bmi1* (a PcG gene) and *Mll1* (a TrxG gene) partially rescue the skeletal transformation phenotype seen in the individual mutants, suggesting epistasis between PcG and TrxG proteins.[4] Later epigenomic studies have shown that H3K27me3 and H3K4me3, which are respectively deposited by PRC2 and TrxG proteins, are formed at thousands of CG-rich developmental gene promoters in mouse embryonic stem cells (mESCs),[5] and it has been proposed that bivalent chromatin poises genes for immediate activation in response to developmental signaling and stimuli. Gene perturbation experiments in mESCs demonstrated that MLL2 depletion causes an increase in PRC2 occupancy and H3K27me3 enrichment, indicating that MLL2 antagonizes PRC2 at bivalent promoters in mESCs.[6,7] Accumulating evidence has shown that bivalent chromatin is also present *in vivo*, including early embryos, gametes, and germ cells.[3,8–17] However, it is unknown how PcG and TrxG proteins counteract to form bivalent chromatin *in vivo* during mammalian development.

Mouse oocytes provide an excellent model to study epigenetic regulation *in vivo*. They arrest their cell cycle at meiotic prophase I and grow in size without cell division or DNA replication for 1–2 months. This period of oogenesis provides a unique opportunity to minimize the confounding effects of gene perturbations that often negatively affect cell cycle and proliferation. Importantly, histone modifications are progressively deposited across chromatin during oocyte growth, including MLL2-deposited H3K4me3, PRC2-deposited H3K27me3, and PRC1-deposited H2AK119ub1.[8,13,18] H3K4me3 and H3K27me3 are colocalized at thousands of CG-rich promoters, forming bivalent chromatin in fully grown oocytes (FGOs).[8] In addition to (or in some regions overlapping with) bivalent promoters, broad H3K27me3 domains are also established during oocyte growth.[13] They are passed on to the early embryo and mediate maternal-allele-specific gene repression in a germline DNA methylation-independent fashion, a mechanism known as noncanonical

Please cite this article in press as: Mei et al., H2AK119ub1-MLL2 counteraction underlies heritable H3K27me3 formation in oocytes, Molecular Cell (2026), https://doi.org/10.1016/j.molcel.2026.03.014

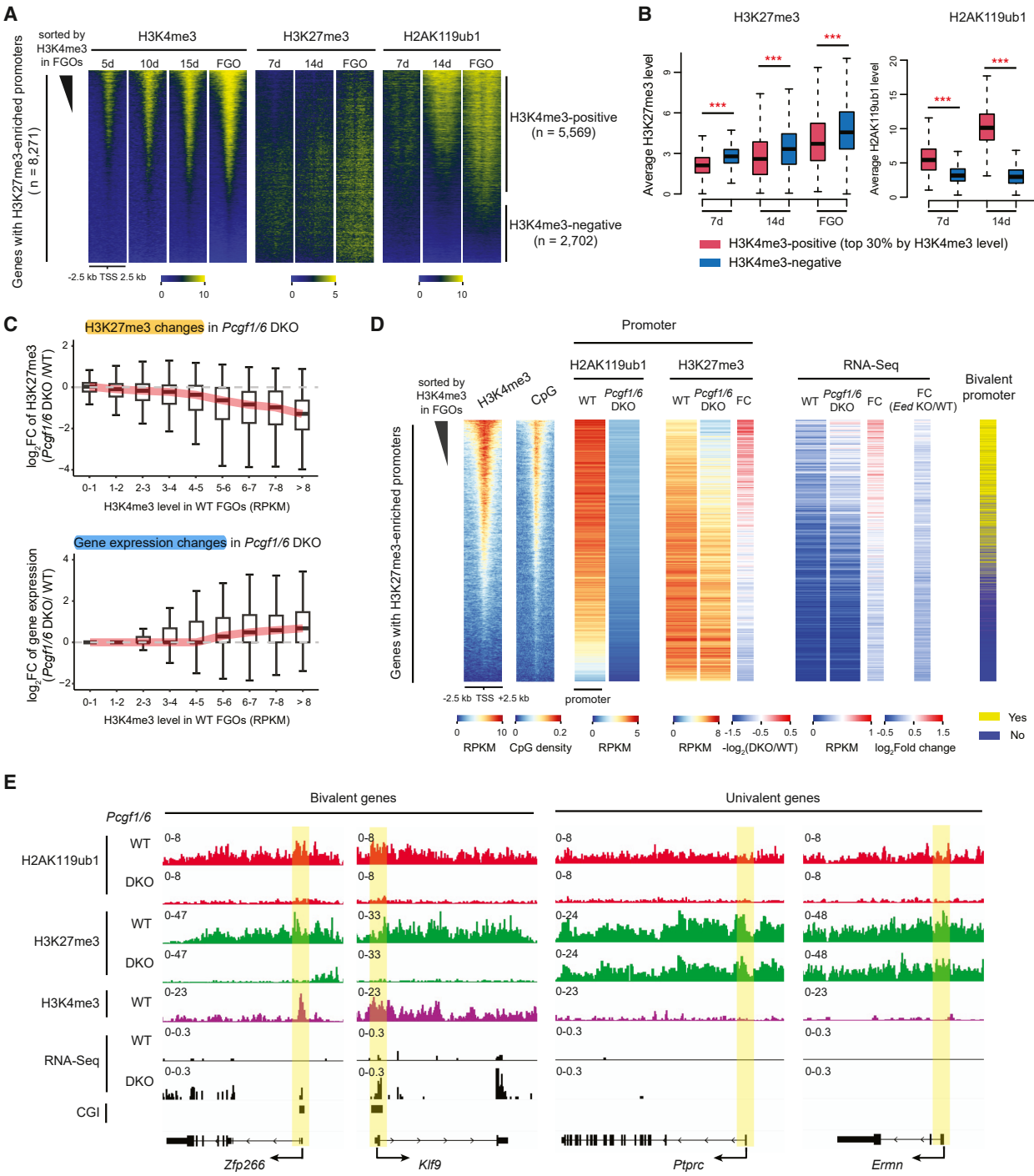

Figure 1. Bivalent genes require H2AK119ub1 for H3K27me3 deposition in mouse oocytes

(A) Heatmaps showing the dynamics of H3K4me3, H3K27me3, and H2AK119ub1 enrichment at promoters of H3K27me3-harboring genes during oocyte growth. H3K4me3-positive genes were defined by average H3K4me3 level (RPKM > 3) at promoters in FGOs. The primary (5–7 days), secondary (10 days), and preantral (14–15 days) stages, as well as the fully grown oocyte (FGO), represent different stages of oocyte growth. H3K4me3, H3K27me3, and H2AK119ub1 datasets are from Hanna et al.,[8] Du et al.,[42] and Mei et al.,[18] respectively.

(B) Boxplots showing the average signal of H3K27me3 and H2KA119ub1 at promoter regions of the top 30% H3K4me3-positive and all H3K4me3-negative genes during oogenesis. The center lines in the boxes represent median values. The box edges and upper and lower whiskers indicate the interquartile range (IQR, from the 25th to 75th percentile), the maximal value smaller than 1.5 × the IQR above the 75th percentile, and the minimal value larger than 1.5 × the IQR below the 25th

(legend continued on next page)

Please cite this article in press as: Mei et al., H2AK119ub1-MLL2 counteraction underlies heritable H3K27me3 formation in oocytes, Molecular Cell (2026), https://doi.org/10.1016/j.molcel.2026.03.014

imprinting.[19,20] Defective deposition of H3K27me3 in oocytes leads to loss of noncanonical imprinting (LOI), embryonic sublethality, and placental overgrowth in offspring.[18,21–23] Thus, maternal H3K27me3 functions in intergenerational epigenetic memory important for the next generation's development. Nevertheless, it is poorly understood how bivalent chromatin and H3K27me3 imprinting domains are formed in oocytes.

To examine the role of H2AK119ub1 in H3K27me3 deposition in oocytes, we previously generated an oocyte-specific *Pcgf1/6* double-knockout (DKO) mouse model.[18] PRC1 consists of the E3 ubiquitin ligase components, RING1A and RING1B, and exists in six different forms—PRC1.1 to PRC1.6—each containing one of the six Polycomb group ring finger (PCGF) proteins, PCGF1 to PCGF6, respectively.[24–26] PRC1.1, PRC1.3, PRC1.5, and PRC1.6, collectively known as variant PRC1 (vPRC1), have high activity for H2AK119ub1 deposition, whereas PRC1.2 and PRC1.4, collectively known as canonical PRC1 (cPRC1), have low activity for H2AK119ub1 deposition and instead mediate Polycomb domain clustering.[27–29] Depletion of PCGF1 and 6, two vPRC1-specific subunits highly expressed in oocytes, led to a substantial reduction in H2AK119ub1 throughout the genome.[18] Consequently, H3K27me3 was lost at a subset of genes in *Pcgf1/6* DKO FGOs, leading to partial LOI and placental overgrowth in offspring.[18] Why vPRC1-deposited H2AK119ub1 is selectively required only at specific genes for H3K27me3 deposition remains unknown.

The necessity of H2AK119ub1 for H3K27me3 deposition is known to be context-dependent.[26] For example, upon H2AK119ub1 depletion, H3K27me3 is nearly fully lost at Polycomb-target loci in mESCs[28,30,31] but is only modestly reduced in human cancer cell lines.[32] Subcomplexes of PRCs do not fully explain this context dependency: PRC2.2 is recruited to CpG islands (CGIs) via its H2AK119ub1-binding ability[25] and could underlie the H2AK119ub1 requirement for H3K27me3 deposition in some contexts.[26,33–36] However, unlike H2AK119ub1-depleted mESCs, PRC2.2-specific KO mESCs show only a modest reduction of H3K27me3 at CGIs,[37,38] raising the possibility that the H2AK119ub1-PRC2.2 pathway is not the sole mechanism of H2AK119ub1-dependent H3K27me3 deposition. Thus, the mechanisms underlying the context-dependent requirement of H2AK119ub1 are not fully understood.

Furthermore, it has been controversial whether H2AK119ub1 per se is critical for PRC1 functions *in vivo*: early studies with the PRC1 catalytic mutant or H2A point mutant flies suggested that PRC1's catalytic activity is dispensable for Polycomb-target gene repression.[39] Concordantly, massive reduction of H2AK119ub1 in a *Ring1b* catalytically hypomorphic mutant in the mouse caused a much milder developmental phenotype when compared with a *Ring1b*-null mutant,[40] arguing against the critical role of H2AK119ub1 in animal development. By contrast, studies in mESCs have shown that the defective Polycomb repression and cell viability seen in a *Ring1a/b*-null mutant are recapitulated by a PRC1 catalytic dead (PRC1-CD) mutant,[30,31] prompting further investigation into whether PRC1 catalytic activity is crucial for mammalian development.

In this study, we find that genes carrying higher basal levels of promoter H3K4me3 are more derepressed and lose more H3K27me3 in *Pcgf1/6* DKO and PRC1-CD mutant oocytes. Importantly, combinatorial depletion of MLL2 abrogates H3K4me3 at many bivalent promoters, restoring transcriptional silencing and H3K27me3 deposition even in an H2AK119ub1-deficient state in *Pcgf1/6/Mll2* triple KO (TKO) oocytes. This restoration also occurs at *Sfmbt2*, a noncanonical imprinted gene hosting the chromosome-2 microRNA cluster (C2MC) crucial for placental development, leading to suppression of maternal-allele expression and placental overgrowth in offspring. Our study thus uncovers that H2AK119ub1 counteracts MLL2-mediated gene activation to confer intergenerationally heritable H3K27me3 during oogenesis. These results suggest that H2AK119ub1 guides H3K27me3 deposition by counteracting MLL2 function and keeping bivalent promoters in a repressed state.

RESULTS

Bivalent genes require vPRC1 for H3K27me3 deposition

To determine putative bivalent chromatin in FGOs, we first conducted unsupervised analyses. ChromHMM[41] analysis revealed that 7.2% of chromatin exhibits bivalent features characterized by the presence of H3K4me3, H3K27me3, and H2AK119ub1 (Figure S1A). K-means clustering identified 5,558 bivalent genes in FGOs, which were characterized by high CpG density and low gene expression levels (Figure S1B; Table S1). Next, we examined the temporal dynamics of these marks during oocyte growth toward H3K27me3 formation. To this end, we defined high-confidence H3K27me3-harboring genes at promoters in FGOs (n = 8,271, see STAR Methods) and aligned them according to the basal levels of promoter H3K4me3 (Figure 1A). We observed that H2AK119ub1 signals at H3K4me3-harboring genes are consistently higher than those at H3K4me3-negative genes across oocyte growth, whereas H3K27me3 shows the opposite trend (Figures 1A, 1B, and S1C). This suggests that H2AK119ub1 and H3K27me3 are deposited at bivalent genes relatively early and late, respectively, during oocyte growth.

To investigate the role of vPRC1-mediated H2AK119ub1 in H3K27me3 deposition, we reanalyzed previous datasets for

percentile, respectively. The same definitions were used in the following boxplots. The p values were calculated by a two-sided Mann-Whitney U test. All p values were less than 2.2e−16 (***).

(C) Boxplots showing the FCs of promoter H3K27me3 and gene expression levels between *Pcgf1/6* WT and DKO FGOs. The red lines in the boxes represent median values.

(D) Heatmaps showing the signal intensities of the indicated histone modifications at promoters of H3K27me3-harboring genes in *Pcgf1/6* WT and DKO FGOs. Each row represents the average levels of the indicated histone modifications within each gene promoter. The rows were sorted by basal H3K4me3 levels of WT FGOs in descending order. The FC in RNA-seq columns indicates the relative gene expression in FGOs ($\log_2$FC [KO/WT]). The rightmost column indicates bivalent genes defined in Figure S1B. The H2AK119ub1 and H3K27me3 CUT&RUN and RNA-seq datasets are from Mei et al.[18] The H3K4me3 ChIP-seq dataset is from Hanna et al.[8] The RNA-seq dataset of *Eed* KO FGOs is from Du et al.[42] (GEO: GSE118263).

(E) Genome browser views of the indicated histone modifications at bivalent and univalent genes. Promoter regions are highlighted in yellow. CGI, CpG island.

Please cite this article in press as: Mei et al., H2AK119ub1-MLL2 counteraction underlies heritable H3K27me3 formation in oocytes, Molecular Cell (2026), https://doi.org/10.1016/j.molcel.2026.03.014

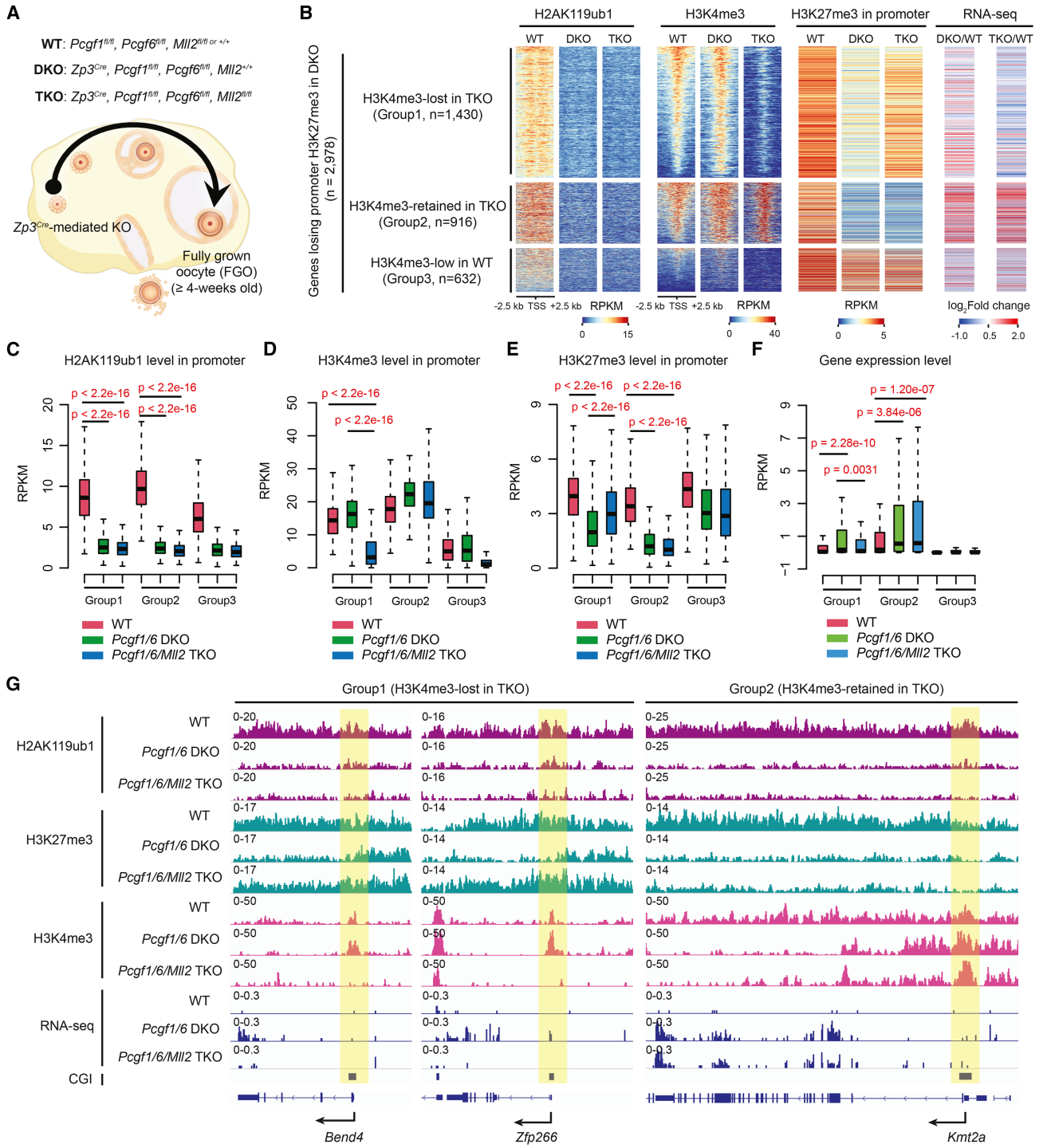

Figure 2. Combinatorial depletion of MLL2 partially restores H3K27me3 in an H2AK119ub1-decifient state

(A) Schematic of the ovary.

(B) Heatmaps showing H2AK119ub1, H3K4me3, and H3K27me3 enrichment at promoters of H3K27me3-lost genes in *Pcgf1/6* DKO. Three groups are defined by H3K4me3 levels. RNA-seq columns indicate the FCs in gene expression levels.

(C–E) Boxplots showing the average signals of H2AK119ub1 (C), H3K4me3 (D), and H3K27me3 (E) at promoters in WT, DKO, and TKO oocytes. The center lines in the boxes represent median values. The box edges and upper and lower whiskers indicate the interquartile range (IQR, from the 25th to 75th percentile), the

(legend continued on next page)

Please cite this article in press as: Mei et al., H2AK119ub1-MLL2 counteraction underlies heritable H3K27me3 formation in oocytes, Molecular Cell (2026), https://doi.org/10.1016/j.molcel.2026.03.014

H2AK119ub1, H3K27me3, and RNA sequencing (RNA-seq) in *Pcgf1/6* DKO FGOs.[18] Interestingly, we found that genes with higher H3K4me3 levels were more transcriptionally derepressed and lost more H3K27me3 in *Pcgf1/6* DKO FGOs (Figures 1C–1E), suggesting that PCGF1/6-vPRC1 is required for H3K27me3 deposition at bivalent genes. To further characterize the epigenetic and genetic features of H3K27me3-lost genes, we next grouped all high-confidence H3K27me3-harboring genes (n = 8,271) according to the extent of H3K27me3 loss at promoters in *Pcgf1/6* DKO FGOs. As a result, 2,978 (36%) genes displayed a robust loss of H3K27me3 (fold change [FC] wild-type [WT]/DKO) > 1.5) (cluster1) and showed higher levels of promoter H3K4me3 and CG density (Figures S1D–S1G). Consistently, 89% (2,664) of the 2,978 were categorized as "bivalent" genes. Gene Ontology (GO) analysis showed that cluster1 and 2 were enriched in developmental- and immune-related genes, respectively (Figure S1H). Transcription factor (TF) motif enrichment analysis at promoters showed unique enrichment of KLF17 in cluster1 (Figure S1I). Reanalysis of RNA-seq confirmed that cluster1 is significantly derepressed in *Pcgf1/6* DKO FGOs (Figures 1D and S1J). Notably, these genes were much less activated in *Eed* KO FGOs than in *Pcgf1/6* DKO FGOs (Figures 1D and S1J), indicating that they are predominantly repressed by vPRC1 but not by PRC2. Indeed, H2AK119ub1 was largely retained at bivalent genes in *Eed* KO FGOs (Figure S1K). Similar analyses of H3K27me3-harboring gene bodies (n = 7,622) showed that 2,553 (33%, cluster1) genes lost H3K27me3, and most of these genes were derepressed in *Pcgf1/6* DKO FGOs (Figures S1L and S1M). These 2,553 genes almost entirely overlapped with the 2,978 genes that lost promoter H3K27me3 (Figure S1N), indicating that H3K27me3 is concurrently lost in promoter and gene body regions, accompanied by gene derepression in the DKO FGOs. These results demonstrate that PCGF1/6-vPRC1 is required for H3K27me3 deposition at both the promoters and gene bodies of bivalent genes.

MLL2 depletion restores H3K27me3 in an H2AK119ub1-deficient state

H3K4me3 at bivalent gene promoters is mainly deposited by MLL2.[3,8] To examine whether MLL2 is causal of transcriptional derepression and H3K27me3 loss in *Pcgf1/6* DKO oocytes, we generated an oocyte-specific *Pcgf1/6/Mll2* TKO mouse model by using an oocyte-specific ZP3^{Cre} driver line.[43] Hereafter, *Pcgf1*$^{fl/fl}$/*Pcgf6*$^{fl/fl}$/*Mll2*$^{fl/fl}$/*Zp3*^{Cre} and *Pcgf1*$^{fl/fl}$/*Pcgf6*$^{fl/fl}$/*Mll2*$^{fl/fl}$ are referred to as TKO and WT, respectively (Figure 2A). Immunostaining analysis confirmed that the H2AK119ub1 level in TKO FGOs is as low as that in *Pcgf1/6* DKO FGOs and that H3K4me3 is greatly reduced in the TKO compared with the WT and DKO (Figure S2A), consistent with the results of previous immunostaining in *Mll2* KO FGOs.[44] Spike-in CUT&RUN analysis also confirmed that H2AK119ub1 is deficient in both DKO and TKO FGOs (Figures 2B, 2C, and S2B).

To determine whether H3K4me3 is successfully depleted from bivalent gene promoters, we performed H3K4me3 carrier DNA-assisted chromatin immunoprecipitation sequencing (CATCH-seq,[33,45] see STAR Methods) with spike-in normalization for WT, DKO, and TKO FGOs using biological duplicates, which showed high reproducibility (Figure S2C). We confirmed that H3K4me3 is greatly reduced at bivalent gene promoters in the TKO (Figure S2D). According to the extent of H3K4me3 changes, the 2,978 genes that had lost promoter H3K27me3 in DKO FGOs (cluster1 in Figure S1D) were clustered into 3 groups (Figure 2B): group1 showed a high level of H3K4me3 in the WT and DKO (RPKM > 4), which was lost in the TKO (FC [TKO/DKO] < 0.5) (Figure 2D). Group2 retained H3K4me3 even in the TKO (RPKM > 4, FC [TKO/DKO] > 0.5), possibly due to compensation by other H3K4 methyltransferases, such as SETD1B.[46,47] Group1 and group2 were similarly enriched in developmental genes (Figure S2E), but several TF motifs, including ZFP652 and NRF1, were uniquely enriched in group1 and group2, respectively (Figure S2F). Group3 (the remaining genes) had relatively lower levels of H3K4me3 in all samples (Figure 2B). Then, we performed H3K27me3 CUT&RUN analysis with spike-in normalization and RNA-seq (Figures S2G and S2H; Table S2). Importantly, both H3K27me3 deposition and gene repression were significantly restored in group1, but not group2, in the TKO (Figures 2B and 2E–2G). Thus, changes in promoter H3K4me3 levels at group1 were highly correlated with transcription and promoter H3K27me3 levels in TKO FGOs. These results suggest that vPRC1 ensures H3K27me3 deposition via antagonizing MLL2-mediated gene activation in oocytes.

We next investigated how H3K27me3 is changed at noncanonical imprinted genes in DKO and TKO FGOs. Of the 35 noncanonical imprinted genes analyzed, 29 showed H3K4me3 enrichment at their annotated transcription start sites (TSSs) in WT FGOs. Among these, 16 displayed a reduction in H3K27me3 levels across their gene bodies in DKO FGOs (Figure S2I). The remaining 13 genes retained H3K27me3, suggesting that residual H2AK119ub1 (as discussed below) and/or other unknown mechanisms might contribute to H3K27me3 deposition. Of the 16 genes that lost H3K27me3 in DKO FGOs, eight, including *Sfmbt2*, showed partial or complete restoration of H3K27me3 in TKO FGOs, which coincided with loss of promoter H3K4me3 and transcriptional repression (Figure S2J). The other eight did not regain H3K27me3, remained derepressed, and continued to display relatively high H3K4me3 levels at their promoters in TKO FGOs (Figure S2J). Thus, a subset of noncanonical imprinted genes exhibited coordinated changes in H3K27me3 and transcription.

The loss of H3K27me3 occurred not only at promoter regions but also across gene bodies in *Pcgf1/6* DKO oocytes (Figure S3A). This observation prompted us to ask why H3K27me3 is lost across gene bodies despite the minimal presence of H3K4me3 in these regions. To this end, we examined the distributions of H3K36me3 and H3K36me2, which are

maximal value smaller than 1.5 × the IQR above the 75th percentile, and the minimal value larger than 1.5 × the IQR below the 25th percentile, respectively. p values (two-tailed Mann-Whitney U test) are also shown.

(F) Boxplots showing the gene expression levels in the WT, DKO, and TKO. p values (two-tailed t test) are also shown.

(G) Genome browser views of the indicated histone modifications and RNA-seq tracks at representative loci of group1 and group2. Promoter regions are highlighted in yellow. CGI, CpG island.

Please cite this article in press as: Mei et al., H2AK119ub1-MLL2 counteraction underlies heritable H3K27me3 formation in oocytes, Molecular Cell (2026), https://doi.org/10.1016/j.molcel.2026.03.014

known to be deposited across transcribed gene bodies and counteract PRCs.[48–53] H3K36me2 is also known to be distributed over intergenic regions.[52,54] Using specific antibodies against H3K36me2[11,52,54,55] and against H3K36me3,[11,51,54,56] we performed CATCH-seq analyses for WT, DKO, and TKO FGOs with biological replicates, which showed high reproducibility (Figures S3B and S3C). Consistent with a previous study,[56] we confirmed that H3K36me2 and H3K36me3 are differentially distributed across the X chromosome in WT FGOs, validating the success of distinct mapping of these two modifications (Figure S3D). For gene body analyses, we focused on the 2,553 genes that lost H3K27me3 across gene bodies in the DKO (cluster1 in Figure S1L), which were almost entirely a subset of the genes that lost promoter H3K27me3 (Figure S1N). By comparing WT and DKO FGOs, we found that both H3K36me2 and H3K36me3 levels were remarkably increased at the bodies of H3K27me3-lost genes in DKO FGOs (cluster1), although they remained low at genes not losing H3K27me3 in the DKO (cluster2) (Figures S3E and S3F). This indicates that H3K27me3 reduction across gene bodies is accompanied by a gain of H3K36me2/3 in *Pcgf1/6* DKO FGOs. According to H3K27me3 restoration levels in TKO FGOs, we then classified cluster1 into 3 groups (Figures 3A and 3B): group1 showed H3K27me3 restoration (FC [DKO/WT] < 0.5, FC [TKO/DKO] > 2), whereas group2 did not (FC [DKO/WT] < 0.5, FC [TKO/WT] < 0.5). Group3 contained the remaining genes, including those mildly losing H3K27me3 in the DKO and those mildly restoring H3K27me3 in the TKO. Importantly, H3K36me2 and H3K36me3 were significantly decreased in group1, but not group2, in *Pcgf1/6/Mll2* TKO FGOs (Figures 3A and 3C–3E). This decrease was not caused by a potential redistribution of H3K4me3, as H3K4me3 remained low across gene bodies of group1 in the TKO (Figure S3G). Furthermore, the gain of H3K36me2 in the DKO was largely restricted to gene bodies (Figures S3H and S3I), suggesting that it may be deposited by transcription-coupled SETD2.[52,54] Taken together, these results suggest that transcription-coupled H3K36me2/3 deposition is likely a cause of H3K27me3 changes across gene bodies in DKO and TKO FGOs. Thus, when MLL2 was depleted and transcription was silenced, H3K27me3 could be deposited at both promoters and gene bodies, even under an H2AK119ub1-deficient condition. This also suggests that vPRC1 mediates H3K27me3 deposition by keeping bivalent promoters in a repressed state.

H3K27me3 restoration in oocytes ameliorates placental overgrowth in offspring

Oocyte-derived H3K27me3 domains mediate noncanonical imprinting, which restricts placental overgrowth.[57] In the offspring derived from *Pcgf1/6* DKO oocytes, an H3K27me3-deficient state is maintained during early development, leading to partial LOI and placental overgrowth at term.[18] To examine whether the placenta is normalized in offspring derived from *Pcgf1/6/Mll2* TKO oocytes, in which H3K27me3 is partially restored, we transferred the chromatin of TKO oocytes into enucleated WT oocytes to bypass the very early developmental lethality reported in *Mll2* maternal KO embryos[44] (Figure 4A). Simultaneously, we carried out chromatin transfer for WT and DKO oocytes as control groups. This procedure allowed us to investigate the chromatin-based intergenerational effects on the offspring. By fertilizing the reconstructed oocytes with WT sperm, we transplanted maternal TKO (matTKO), maternal DKO (matDKO), and WT embryos into surrogate mothers, and performed C-section at term (E18.5). Consistent with our previous study,[18] some of the matDKO offspring had enlarged placentae (Figure 4B). Remarkably, none of the matTKO offspring showed placental overgrowth (Figure 4B). Periodic Acid Schiff (PAS) staining of placental sections demonstrated that enlargement of the spongiotrophoblast (ST) layer, a histological hallmark of overproliferation of fetal-derived placental cells, is normalized in the matTKO placentae (Figures 4C and S4A).

By heterozygous KO screening of individual noncanonical imprinted genes in a LOI model, namely *Eed* matKO embryos, we previously identified *Sfmbt2* and *Slc38a4* as the key genes responsible for placental overgrowth.[22] To examine whether either or both of these genes show LOI in *Pcgf1/6* matDKO embryos, which is restored in *Pcgf1/6/Mll2* matTKO embryos, we performed allelic RNA-seq analysis for ten each of WT, matDKO, and matTKO morula embryos of a hybrid strain. We found that the maternal allele of *Sfmbt2* is derepressed in some matDKO embryos, but this was less apparent in matTKO embryos (Figure 4D; Table S3). By contrast, *Slc38a4* was kept silenced in matDKO embryos (Figure S4B). Visual inspection of H3K27me3 distribution at *Sfmbt2* revealed a modest decrease in DKO FGOs and restoration in TKO FGOs (Figure 4E). Consistently, *Sfmbt2* lost promoter H3K4me3 in the TKO, was derepressed in the DKO but silenced in the TKO, and gained H3K36me2/3 in the DKO but not in the TKO (Figure 4E). Although H3K36me3 levels increased in the DKO, they remained relatively low, likely because the low transcriptional activity was insufficient to fully methylate H3K36.[54] In contrast, *Slc38a4* did not exhibit a reduction of H3K27me3, gain of H3K36me2/3, or transcriptional derepression in the DKO, consistent with the fact that it lacks promoter H3K4me3 in WT FGOs (Figure S4C).

Sfmbt2 harbors the C2MC in intron 10, which has few mapped sequencing reads due to its repeat nature (Figure 4E). Because C2MC is processed from *Sfmbt2* mRNA, LOI of *Sfmbt2* also causes LOI of C2MC.[58] We and others have previously demonstrated that LOI-mediated biallelic expression of C2MC causes placental overgrowth in *Eed* matKO offspring and cloned mice.[22,59] To determine whether LOI of C2MC is a cause of placental overgrowth in *Pcgf1/6* matDKO offspring, we generated *Pcgf1/6*/C2MC TKO oocytes by deleting the C2MC in the *Pcgf1*$^{fl/fl}$/*Pcgf6* $^{fl/fl}$/*Zp3*^{Cre} mouse line (Figure S4D). Fertilization with WT sperm and embryo transplantation, followed by C-section at term, revealed that placental overgrowth was ameliorated in the *Pcgf1/6*/C2MC matTKO offspring when compared with the *Pcgf1/6* matDKO offspring (Figures 4F and S4E–S4G). These results not only demonstrate that C2MC is the key imprinting locus responsible for placental overgrowth in *Pcgf1/6* matDKO offspring but also suggest that even slight loss of H3K27me3 at *Sfmbt2* in oocytes can have long-term consequences for the next generation's development.

PRC1 catalytic activity is crucial for H3K27me3 deposition at bivalent genes in oocytes

Because it is not known whether H2AK119ub1 per se is the pivotal determinant of PRC1 functions and required for

Please cite this article in press as: Mei et al., H2AK119ub1-MLL2 counteraction underlies heritable H3K27me3 formation in oocytes, Molecular Cell (2026), https://doi.org/10.1016/j.molcel.2026.03.014

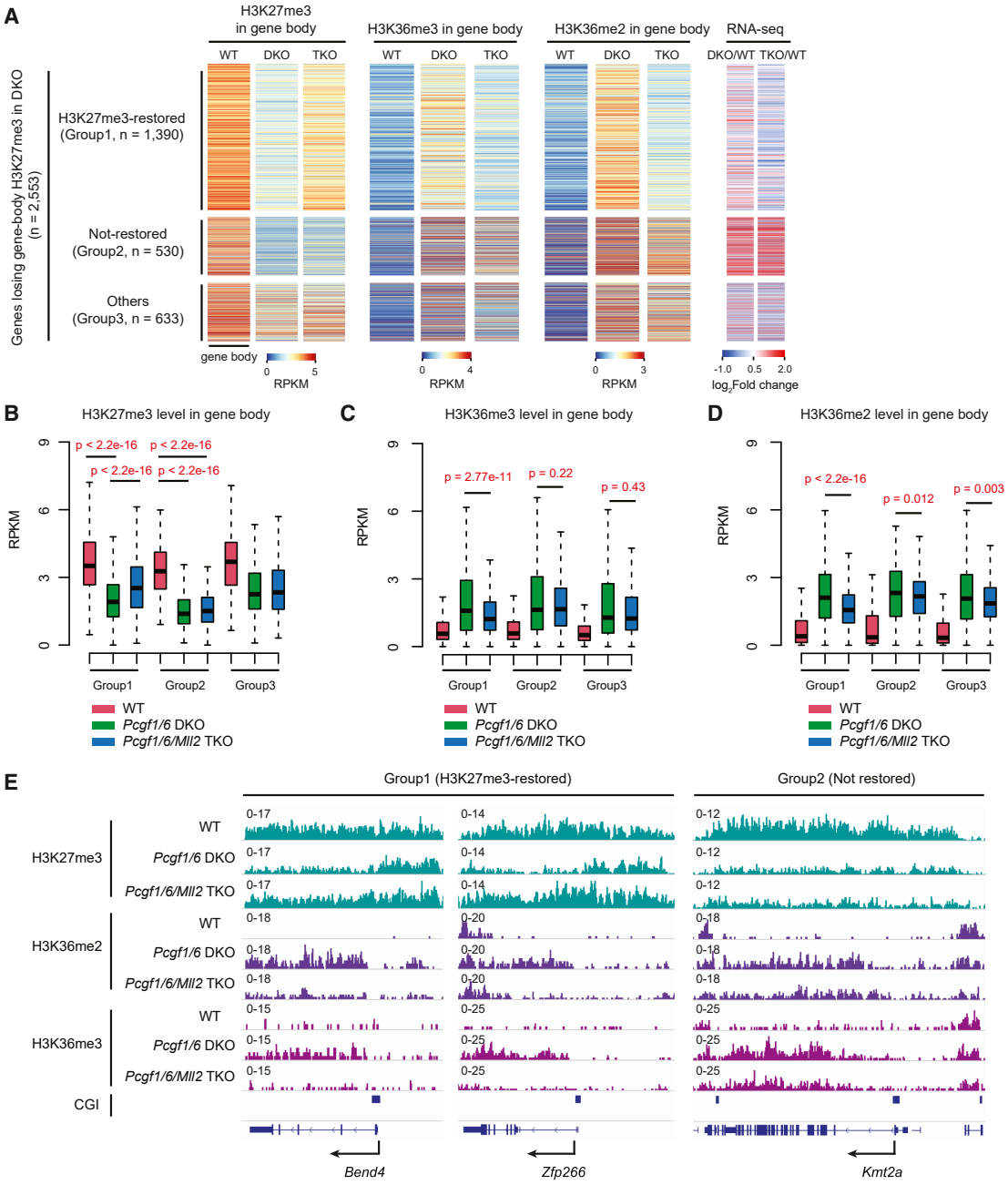

Figure 3. Loss of H3K27me3 across gene bodies is associated with gain of H3K36me2/3

(A) Heatmaps showing the average levels of H3K27me3, H3K36me3, and H3K36me2 enrichment across gene bodies of H3K27me3-lost genes in *Pcgf1/6* DKO. Three groups are defined by H3K27me3 restoration levels. RNA-seq columns indicate the FCs in gene expression levels.

(B–D) Boxplots showing the average H3K27me3 (B), H3K36me3 (C), and H3K36me2 (D) signals in gene bodies. The *p* values were calculated by a two-sided Mann-Whitney *U* test.

(E) Genome browser views of representative loci of group1 and group2. CGI, CpG island.

H3K27me3 deposition *in vivo* during mammalian development, we sought an answer to this question in oocytes. To this end, we generated PRC1-CD mutant oocytes by using a *Ring1b* I53A/D56K conditional point mutant allele (Figure S5A)[30] crossed with a *Ring1a*$^{-/-}$ line and an oocyte-specific ZP3^{Cre} driver line.[43] Immunostaining analysis confirmed that H2AK119ub1 is completely abolished and H3K27me3 is significantly reduced in PRC1-CD FGOs (Figure 5A). We then performed H3K27me3 CATCH-seq with biological duplicates that showed high reproducibility (Figure S5B). The result showed that genes with higher

Please cite this article in press as: Mei et al., H2AK119ub1-MLL2 counteraction underlies heritable H3K27me3 formation in oocytes, Molecular Cell (2026), https://doi.org/10.1016/j.molcel.2026.03.014

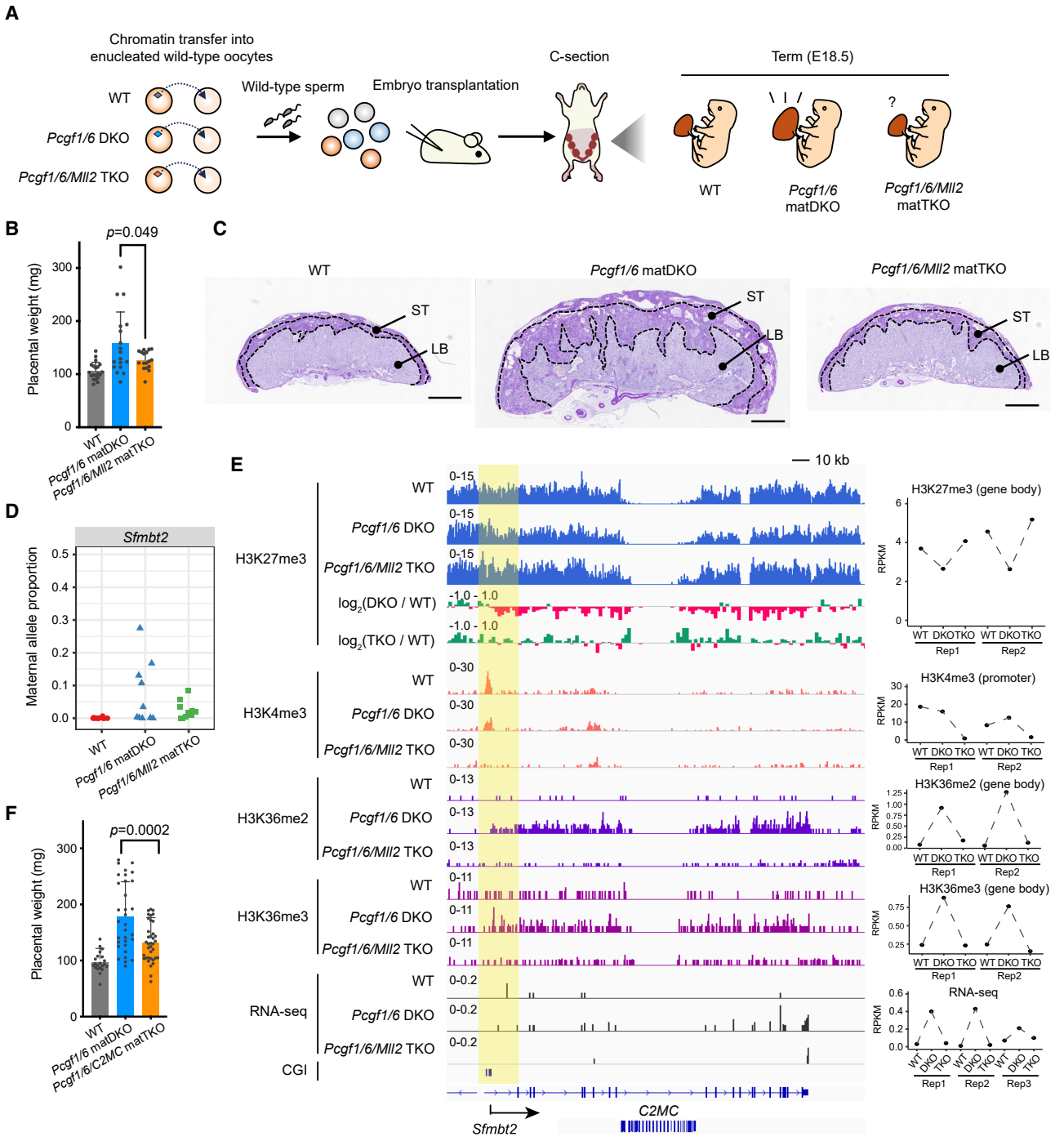

Figure 4. H3K27me3 restoration in oocytes leads to amelioration of placental overgrowth in offspring

(A) Experimental scheme to assess the intergenerational effects of epigenetic changes in oocytes.

(B) Placental weights of WT, *Pcgf1/6* matDKO, and *Pcgf1/6/Mll2* matTKO offspring at E18.5. The numbers of placentae examined were 20 (WT), 18 (*Pcgf1/6* matDKO), and 17 (*Pcgf1/6/Mll2* matTKO). These were derived from 7 litters with 5–11 fetuses per litter.

(C) Representative images of placental sections with PAS staining. LB, labyrinthine layer; ST, spongiotrophoblast layer. The number of placentae dissected were 3 (WT), 3 (*Pcgf1/6* matDKO), and 4 (*Pcgf1/6/Mll2* matTKO). Scale bars, 1 mm.

(D) Scatterplot showing the maternal-allele proportion of *Sfmbt2* gene expression in morula embryos. Each dot represents a single embryo ($n = 10$ each). Values of 0.0 and 0.5 indicate that 0% and 50% of RNA-seq reads, respectively, of *Sfmbt2* are derived from the maternal allele.

(legend continued on next page)

Please cite this article in press as: Mei et al., H2AK119ub1-MLL2 counteraction underlies heritable H3K27me3 formation in oocytes, Molecular Cell (2026), https://doi.org/10.1016/j.molcel.2026.03.014

levels of promoter H3K4me3 in WT FGOs lose more H3K27me3 in PRC1-CD FGOs (Figures 5B–5D). RNA-seq analysis confirmed that these genes are derepressed in PRC1-CD FGOs (Figures 5B–5D). Both derepressed genes and H3K27me3-lost genes in PRC1-CD FGOs highly overlapped with those in *Pcgf1/6* DKO FGOs (Figures 5C, S5C, and S5D). These data strongly suggest that H3K27me3 deposition at bivalent gene promoters is H2AK119ub1-dependent and show that promoter H3K4me3 levels can predict the necessity of H2AK119ub1 for H3K27me3 deposition in oocytes. Curiously, we observed that the extent of gene derepression and H3K27me3 loss in the PRC1-CD mutant is greater than that in the *Pcgf1/6* DKO (Figures 5C, S5C, and S5D). This was also evident for noncanonical imprinted genes, some of which lost H3K27me3 only in PRC1-CD, but not *Pcgf1/6* DKO, FGOs (Figure S5E). These observations suggest that residual H2AK119ub1 may still exert some repressive effects, reminiscent of *Pcgf1/3/5* TKO mESCs in which H2AK119ub1 is markedly reduced, yet repressive activity is partially retained.[28] Indeed, in *Pcgf1/6* DKO FGOs, it was detectable across regions originally enriched for H2AK119ub1 in WT FGOs (Figure S5F).

Next, to determine whether the PRC1-CD phenotypically recapitulates PRC1-null oocytes, we conducted comparative analyses between PRC1-CD and *Ring1a/b* DKO FGOs.[42] RNA-seq analyses revealed that sets of differentially expressed genes (DEGs), particularly those upregulated, show a high degree of overlap in both mutant FGOs (Figures S5G and S5H; Table S4). Consequently, the great majority of zygotes derived from PRC1-CD oocytes arrested at the 1- or 2-cell stages, and only a very few embryos reached the blastocyst stage (Figure S5I), echoing the phenotypes of *Ring1a/b* matDKO embryos.[60] These data provide the first *in vivo* evidence that the catalytic activity of PRC1 is critical for PRC1 functions in mammals.

Lastly, to examine whether bivalent genes require H2AK119ub1 to form H3K27me3 in other types of cells, we reanalyzed public datasets of mouse spermatogonial stem cells and two human cancer cell lines, HAP1 and DLD-1, all of which contained H2AK119ub1 and H3K4me3 profiles in WT conditions and H3K27me3 profiles in *Ring1a/b* WT and DKO conditions.[9,32] We found two clusters of H3K27me3/H2AK119ub1-harboring promoters in spermatogonial stem cells (Figures S6A–S6D), DLD-1 (Figures S6E–S6H), and HAP1 (Figures S6I–S6L): cluster1 had H3K4me3 peaks at promoters in WT conditions, whereas cluster2 did not. Notably, the great majority of cluster1 promoters lost H3K27me3 in *Ring1a/b* DKO conditions in all these cell types (Figures S6A–S6L). By contrast, only a small portion of cluster2 lost H3K27me3. A detailed correlation analysis confirmed that genes with higher basal levels of promoter H3K4me3 tend to lose more H3K27me3 in DKO conditions in all three cell types (Figures S6C, S6G, and S6K). These data support the notion that H2AK119ub1 is required for H3K27me3 deposition at bivalent genes, echoing the observation in oocytes.

DISCUSSION

PcG and TrxG counteraction in oocytes

Bivalent chromatin is present in various cell types in developing organisms, yet it has remained unknown how PcG and TrxG proteins counteract *in vivo* in mammals and how H2AK119ub1 is required for H3K27me3 deposition in oocytes. In this study, we found that the extent of both H3K27me3 loss and gene derepression upon loss of H2AK119ub1 is proportional to the basal levels of promoter H3K4me3 (Figure 6A, left and middle). H3K27me3 was lost at both promoters and gene bodies, with the latter associated with the deposition of H3K36me2/3, which are known to counteract PRCs.[48–53,61] Meanwhile, non-bivalent genes remained transcriptionally silent and could form H3K27me3 regardless of whether H2AK119ub1 was present or not (Figure 6A, right). This may be attributed to the lack of cognate activating factors (e.g., TFs) at these genes, permitting promiscuous deposition of H3K27me3 over transcriptionally inactive regions in non-dividing oocytes.[13] Additional depletion of MLL2 caused loss of promoter H3K4me3 at many bivalent genes, resulting in substantial recovery of a transcriptional repressive state, loss of H3K36me2/3 deposition, and restoration of H3K27me3 at both promoters and gene bodies in an H2AK119ub1-deficient condition in *Pcgf1/6/Mll2* TKO oocytes (Figure 6A, bottom). This suggests that H2AK119ub1 mediates H3K27me3 deposition primarily by keeping bivalent promoters in a repressed state rather than through direct recruitment of PRC2.2 in oocytes.

Based on these observations, we propose a balanced model in which vPRC1 counteracts MLL2 functions to maintain a repressive state, allowing PRC2 to deposit H3K27me3 (Figure 6B). This model posits a "transcriptional state" as a mediator of vPRC1 and PRC2. The importance of transcriptional states for PRC2 regulation is supported by mESC studies demonstrating that an artificially integrated inactive CGI can recruit PRC2,[62,63] that forced transcription of a transgene cassette causes PRC2 dissociation,[64] and that chemical inhibition of transcription or TSS deletion results in H3K27me3 deposition at some CGIs and a gene body.[35,64,65] Although it is difficult to directly test this idea because prolonged transcriptional inhibition is not feasible in oocytes as it causes cell death, our study not only extends these previous reports to an *in vivo* context but also effectively integrates vPRC1, MLL2, and PRC2 into a simple framework (Figure 6B). This model is applicable to any PRC2 forms. Yet, it does not exclude the possibility that the H2AK119ub1-PRC2.2 pathway plays a role in H3K27me3 deposition in oocytes, as H3K27me3 was not fully restored in the TKO FGOs. Future studies could clarify this point by generating PRC2.2-specific KO oocytes. It is also

(E) Genome browser views of the indicated histone modifications and RNA-seq tracks of the *Sfmbt2*/C2MC locus. The $\log_2$ FCs of H3K27me3 levels (DKO/WT and TKO/WT) are also shown in the 4th and 5th lines. Note that the chromosome-2 microRNA cluster (C2MC) has few sequence reads due to its repeat nature. Line plots on the right indicate the signal values of the indicated histone modifications and RNA-seq in each replicate.
(F) Placental weights of WT, *Pcgf1/6* matDKO, and *Pcgf1/6*/C2MC matTKO offspring at E18.5. The numbers of placentae examined were 21 (WT), 32 (*Pcgf1/6* matDKO), and 37 (*Pcgf1/6*/C2MC matTKO). These were derived from 13 litters with 4–12 fetuses per litter.

Please cite this article in press as: Mei et al., H2AK119ub1-MLL2 counteraction underlies heritable H3K27me3 formation in oocytes, Molecular Cell (2026), https://doi.org/10.1016/j.molcel.2026.03.014

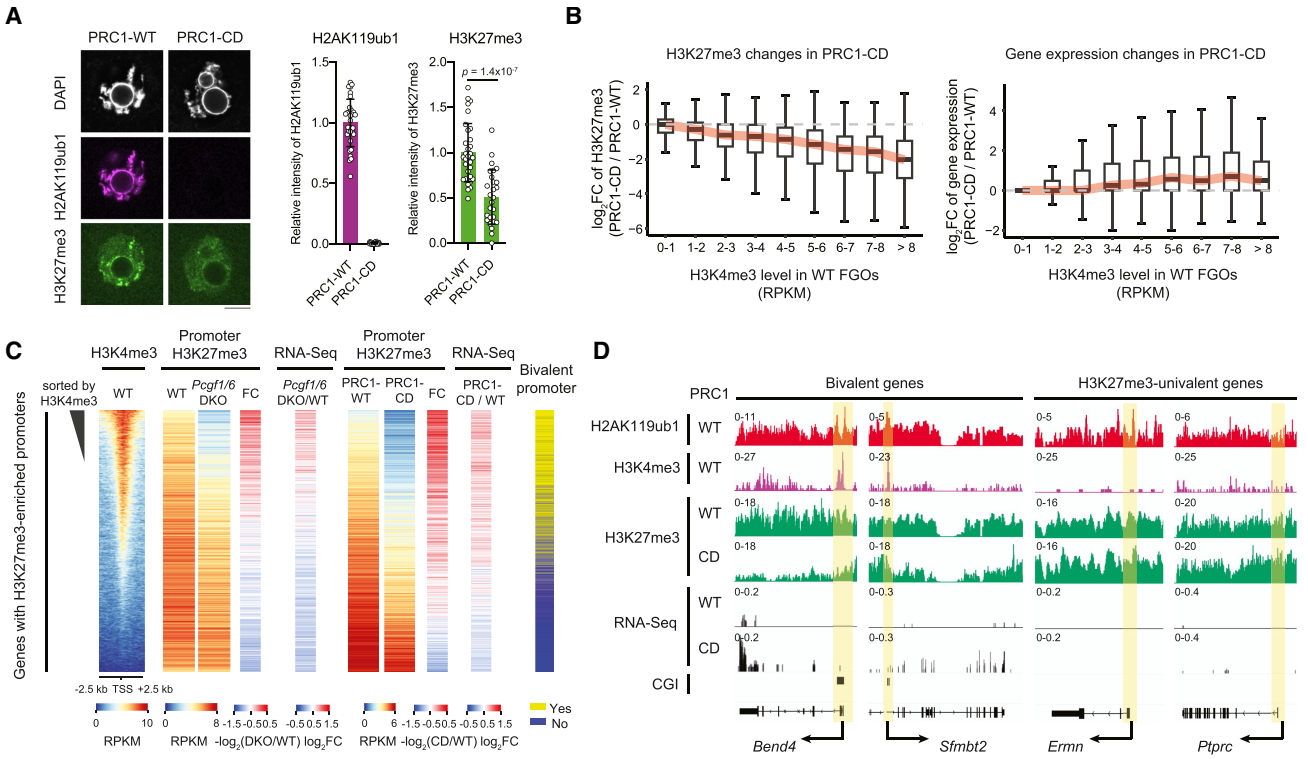

Figure 5. PRC1 catalytic activity is crucial for H3K27me3 deposition at bivalent genes in oocytes

(A) Representative images and quantification of FGOs immunostained with anti-H2AK119ub1 and H3K27me3 antibodies. The average signals of WT were set as 1.0. The total number of FGOs examined in three independent experiments was 32 (WT) and 27 (PRC1-CD). CD, catalytic dead; *p*, two-tailed Student's *t* test.

(B) Boxplots showing the FC of promoter H3K27me3 and gene expression levels between PRC1-CD and WT FGOs. The red lines in the boxes represent median values.

(C) Heatmaps showing the level of H3K4me3 and H3K27me3 at promoters of all high-confidence H3K27me3-harboring genes. The RNA-seq column indicates the FC of gene expression. The rows are sorted by basal H3K4me3 levels in descending order.

(D) Genome browser views of the indicated histone modifications at bivalent and H3K27me3-univalent genes. Promoter regions are highlighted in yellow. The H2AK119ub1 in WT FGOs is from Mei et al.[18] (*Pcgf1/6* WT). The H3K4me3 in WT FGOs is from this study (*Pcgf1/6/Mll2* WT).

noteworthy that MLL2-driven transcriptional activation is only appreciated upon loss of H2AK119ub1, which can explain why loss of H3K4me3 did not cause concomitant transcriptional dysregulation in *Mll2* KO oocytes.[8] Furthermore, because the prevalence of promoter H3K4me3 is varies across cell types,[66–69] this model can at least partly explain the context-dependent, gene-selective, and cell-type-specific necessity of H2AK119ub1 for H3K27me3 deposition.

Regarding how H2AK119ub1 mechanistically represses transcription, a recent study using acute PRC1 depletion followed by high-resolution live imaging demonstrated that PRC1-H2AK119ub1 blocks the binding of factors involved in early pre-initiation complex (PIC) formation,[70] but not the pause-release of RNA polymerases.[71] H3K4me3 is known to promote PIC formation.[72] Therefore, we speculate that H2AK119ub1 antagonizes H3K4me3-promoted PIC formation, which might allow PRC2 to stably bind at promoters and fully catalyze H3K27. Regarding the role of H3K4me3, it is known that H3K4me3 can directly inhibit PRC2 binding via inhibition of SUZ12 binding to the H3 tail[49] and its engagement with the EED pocket.[73] Nevertheless, our study could not clarify whether H3K4me3 per se is crucial for antagonizing PRC2 in oocytes. Because it has been suggested that several factors associated with transcription, such as H3K36me3, KDM6, and CBP, are redundantly involved in counteracting PRC2,[74,75] H3K4me3 itself may not be the sole determinant of PRC2 antagonism in oocytes. As it has been debated whether and how H3K4me3 causally directs transcription,[76–78] it will be important in the future to distinguish between the enzymatic and non-enzymatic functions of MLL2 in PRC2 antagonism and determine whether H3K4me3 per se is an integral part of our balanced model.

The observed link between gain of H3K36me2/3 and loss of H3K27me3 across gene bodies remains correlative in our study. However, the causal relationship is supported by several lines of evidence. For example, PRC2 activity is greatly impaired on nucleosome substrates with premethylated H3K36 *in vitro*[48,49]; H3 tails containing H3K36me3 poorly engage with PRC2, impairing PRC2-chromatin interaction *in vitro*[73]; and H3K27me3 invades H3K36me3-premarked regions in *Setd2* KO FGOs.[51] Although experimental validation is required, it is thus likely that ectopic H3K36me2/3 precludes H3K27me3 deposition across the bodies of derepressed genes

Please cite this article in press as: Mei et al., H2AK119ub1-MLL2 counteraction underlies heritable H3K27me3 formation in oocytes, Molecular Cell (2026), https://doi.org/10.1016/j.molcel.2026.03.014

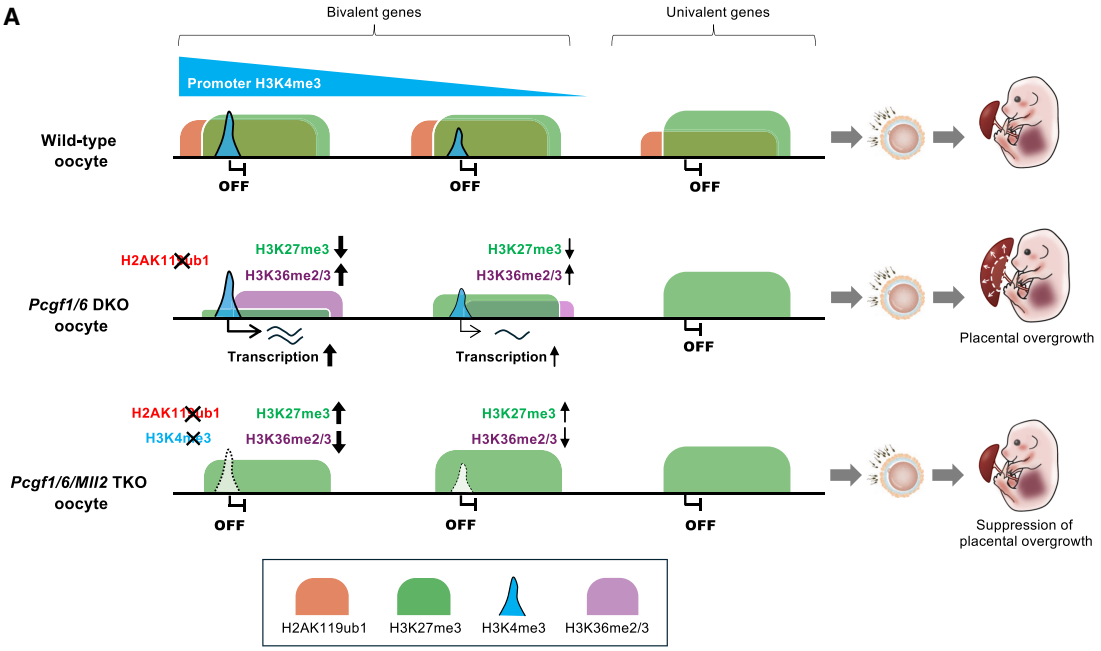

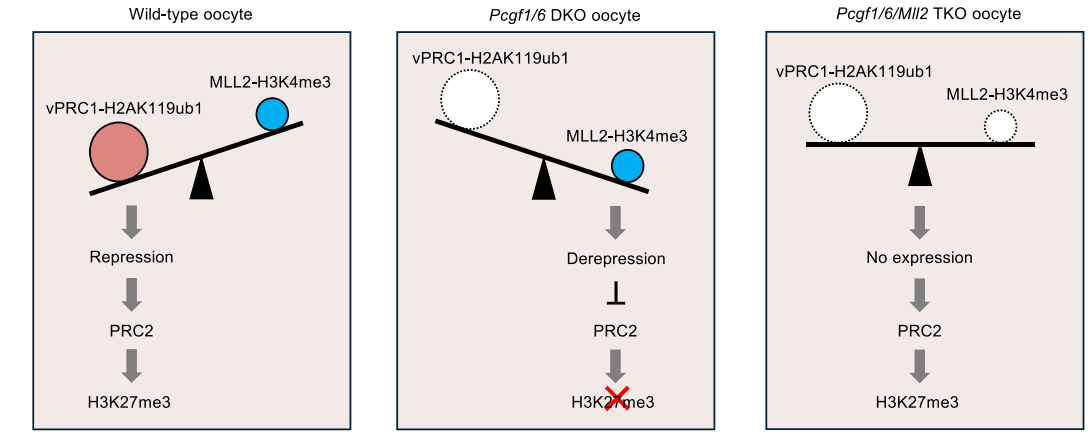

Figure 6. Illustration summary

(A) Summary of epigenetic changes in mutant oocytes. In wild-type oocytes, bivalent genes possessing promoter H3K4me3 are repressed by vPRC1-deposited H2AK119ub1 (left and middle). Under H2AK119ub1 deficiency in *Pcgf1/6* DKO oocytes, they are derepressed, gain gene body H3K36me2/3, and lose H3K27me3, the extent of which is proportional to the basal levels of H3K4me3. Upon additional depletion of MLL2, loss of promoter H3K4me3 is coupled with transcriptional silencing, loss of H3K36me2/3, and restoration of H3K27me3 in *Pcgf1/6/Mll2* TKO oocytes. By contrast, genes without promoter H3K4me3 remain silent, even in the absence of H2AK119ub1, enabling PRC2 to promiscuously deposit H3K27me3 (right). The changes of H3K27me3 in oocytes cause an intergenerational effect on placental development in offspring.

(B) Balance model between PcG and TrxG in mouse oocytes. Bivalent genes carrying H3K27me3 and H3K4me3 are regulated by the balance between vPRC1 and MLL2. In wild-type oocytes (left), vPRC1 is dominant and represses genes, which allows PRC2 to deposit H3K27me3. In *Pcgf1/6* DKO oocytes (middle), MLL2 is dominant and promotes gene expression, which prevents PRC2-mediated H3K27me3 deposition, possibly via antagonistic functions of transcription, H3K4me3, and H3K36me2/3, against PRC2 activity. In *Pcgf1/6/Mll2* TKO oocytes (right), genes are no longer expressed or gain H3K36me2/3, allowing PRC2-mediated H3K27me3 deposition.

in *Pcgf1/6* DKO FGOs. Additionally, other factors associated with RNA polymerase II (RNA Pol II) progression, including KDM6B,[75,79] which is expressed in oocytes,[80] may also contribute to H3K27me3 loss.

Context-dependent mechanisms of bivalent gene repression in development

Which PRC1 or PRC2 complex represses bivalent genes seems to be cell-type specific. For example, bivalent genes are

Please cite this article in press as: Mei et al., H2AK119ub1-MLL2 counteraction underlies heritable H3K27me3 formation in oocytes, Molecular Cell (2026), https://doi.org/10.1016/j.molcel.2026.03.014

derepressed upon PRC2 depletion in adult tissues,[67] which is the case for vPRC1 in mESCs.[81] We show that bivalent genes in oocytes are repressed by vPRC1, but much less so by PRC2, implying that bivalent gene repression relies on vPRC1 in oocytes and early embryos and then shifts to PRC2 by adulthood. This idea is supported by genetic evidence showing that maternal KO of *Ring1a/b*, but not PRC2 core proteins, causes very early lethality[21,60] and that PCGF2/4-cPRC1, an effector of H3K27me3, is dispensable for development until embryonic day (E)8.5 yet is required for neurogenesis thereafter.[28,82–84] Given that the chromatin binding of vPRC1 is highly dynamic and the turnover rate of H2AK119ub1 is much faster than that of H3K27me3,[71,85] a vPRC1-mediated repression system might be beneficial for retaining high chromatin plasticity in totipotent and pluripotent cells.

Insight into intergenerational epigenetic inheritance

Our analysis of *Pcgf1/6*/C2MC matTKO offspring indicated that LOI at C2MC is mainly responsible for placental overgrowth in *Pcgf1/6* matDKO offspring. The magnitude of maternal-allele expression of *Sfmbt2*, the host gene of C2MC, was modest and variable among individual *Pcgf1/6* matDKO embryos at the morula stage. This was in line with the observation that the extent of H3K27me3 loss is also modest in *Pcgf1/6* DKO oocytes and that only some of the matDKO offspring show placental overgrowth. We speculate that H3K27me3 levels might be variable among individual DKO oocytes, leading to variable magnitudes of LOI among individual offspring. The reason that even partial LOI can eventually cause a drastic phenotype in the placentae may be related to a unique maintenance mechanism of noncanonical imprinting, which involves a complex epigenetic cascade: the H3K27me3 primary imprinting mark is taken over by secondary DNA methylation after implantation.[57] During the H3K27me3-to-DNA methylation transition, H3K4me3 deposited at the expressed paternal allele is proposed to block DNMT3A/3B recruitment to escape from *de novo* DNA methylation.[86] Therefore, even modest gene expression may be coupled with H3K4me3 deposition at the maternal allele in preimplantation embryos, which is sufficient to prevent *de novo* DNA methylation and cause LOI and placental overgrowth. In support of this notion, we observed H3K4me3 enrichment at the maternal allele of *Pcgf1/6* matDKO, but not at that of WT, blastocyst embryos (Figure S6M). Thus, our study implies that even apparently modest changes in H3K27me3 memory in oocytes could have long-term consequences for the next generation's development. This concept will contribute to future investigations into how environmental cues might modulate the oocyte epigenome and intergenerationally impact the offspring.

Understanding the biological meaning of bivalent chromatin in oocytes awaits future studies. Although broad H3K27me3 domains are mostly maintained, H3K27me3 at many bivalent promoters is lost after fertilization.[3,11,13] Curiously, this loss is concurrent with transient RNA Pol II installation in zygotes,[87] which is seemingly associated with nascent transcription during minor zygotic genome activation (ZGA).[88] Although it is unknown whether maternally transmitted H3K4me3 plays a role in minor ZGA, it is tempting to speculate that H3K4me3 at bivalent promoters in oocytes primes for minor ZGA. Further understanding of bivalent gene regulation during the maternal-to-zygotic transition will shed light on the hidden functions of bivalent chromatin.

Limitations of the study

Although our results show that MLL2 depletion can bypass the requirement for H2AK119ub1 in H3K27me3 deposition, several mechanistic questions remain unresolved. First, it is unclear whether the antagonism of PRC2 activity in oocytes results directly from H3K4me3 itself or from the non-enzymatic functions of MLL2. Second, it remains to be determined whether transcriptional repression alone is sufficient to restore H3K27me3. Third, the link between gain of H3K36me2/3 and loss of H3K27me3 across gene bodies remains correlative in this study.

RESOURCE AVAILABILITY

Lead contact

Further information and requests for resources and reagents should be directed to the lead contact, Azusa Inoue (azusa.inoue@riken.jp).

Materials availability

Reagents generated in this study will be shared by the lead contact upon request.

Data and code availability

- All sequencing datasets generated in this study have been deposited in the GEO database under accession numbers GEO: GSE292333 and GEO: GSE292237. The H2AK119ub1 and H3K27me3 CUT&RUN and RNA-seq datasets of *Pcgf1/6* CTR and DKO FGOs are available under GEO: GSE153496.[18] The H3K4me3 ChIP-seq datasets of WT FGOs are available under GEO: GSE93941.[8] The RNA-seq datasets of *Eed* KO and *Ring1a/b* DKO FGOs are available under GEO: GSE118263 and GEO: GSE132156,[42] respectively. The H2AK119ub1 CUT&RUN data in *Eed* KO FGOs are available under GEO: GSE153531.[89]
- This paper does not report original code.
- Any additional information required to reanalyze the data reported in this paper is available from the lead contact upon request.

ACKNOWLEDGMENTS

We would like to thank Drs. Satoshi Namekawa (UC Davis), Shinsuke Ito (RIKEN), and Osamu Masui (Ehime Univ), as well as the Inoue lab members, for critical reading of the manuscript; Dr. Taichi Noda (Kumamoto Univ) for advice on the flox knockin construct; RIKEN BRC for providing the JF1 mouse line; Dr. Robert J. Klose (Univ Oxford) for providing the *Ring1b* CPM KI vector; and Dr. Steven Henikoff for providing protein A-MNase for CUT&RUN. This project was partly supported by the Ministry of Education, Culture, Sports, Science, and Technology (MEXT) Grant-in-Aid for Scientific Research on Innovative Areas (19H05754 to A.I.), Grant-in-Aid for Transformative Research Area(A) (25H01355 to A.I.), Grant-in-Aid for Scientific Research (23K27093 to A.I., 23K28009 to C.K., and 24H00563 to H.K.), the Japan Agency for Medical Research and Development PRIME (JP20gm6110012 to A.I.), the JST FOREST Program (JPMJFR2335 to A.I.), the Moonshot R&D Program (JP22zf0127008 to H.K.), and intramural grants within RIKEN, including the RIKEN Pioneering Project "Genome Building from TADs" (to A.I. and H.K.) and "Long-timescale Molecular Chronobiology" (to A.I.).

AUTHOR CONTRIBUTIONS

H.M. and A.I. conceived the project and designed the experiments. C.K., M.K., and A.I. performed the experiments. H.M. analyzed all sequence data. H.M. and A.I. interpreted the data. H.K. provided the *Pcgf1* flox, *Pcgf6* flox, *Ring1a*-null, and *Ring1b*^{CPM} mouse lines. H.M. and A.I. wrote the manuscript.

DECLARATION OF INTERESTS

The authors declare no competing interests.

STAR★METHODS

Detailed methods are provided in the online version of this paper and include the following:

- KEY RESOURCES TABLE
- EXPERIMANTAL MODEL AND STUDY PARTICIPANT DETAILS
  - Mice
- METHOD DETAILS
  - Generation of oocyte-specific *Pcgf1/6/Mll2* conditional triple KO mice
  - Generation of oocyte-specific *Pcgf1/6/C2MC* conditional triple KO mice
  - Generation of oocyte-specific PRC1 catalytic dead (PRC1-CD) mice
  - Collection and culture of mouse oocytes and preimplantation embryos
  - Chromatin transfer
  - Embryo transplantation, Caesarian section, and placental histology
  - Whole mount immunostaining
  - Carrier Assisted ChIP-seq (CATCH-seq)
  - CUT&RUN
  - RNA-seq
- QUANTIFICATION AND STATISTICAL ANALYSIS
  - Low-input chromatin profiling data analyses
  - RNA-seq data analyses
  - Identification of high-confidence H3K27me3-harboring genes
  - Comparison of histone modification at promoters and gene bodies in WT and mutants
  - Transcription factor motif enrichment and Gene ontology analysis
  - Chromatin states analysis and genomic annotation analysis
  - Analysis of publicly available data

SUPPLEMENTAL INFORMATION

Supplemental information can be found online at https://doi.org/10.1016/j.molcel.2026.03.014.

Received: June 2, 2025
Revised: November 25, 2025
Accepted: March 16, 2026

REFERENCES

1. Piunti, A., and Shilatifard, A. (2016). Epigenetic balance of gene expression by Polycomb and COMPASS families. Science *352*, aad9780. https://doi.org/10.1126/science.aad9780.
2. Schuettengruber, B., Bourbon, H.M., Di Croce, L., and Cavalli, G. (2017). Genome Regulation by Polycomb and Trithorax: 70 Years and Counting. Cell *171*, 34–57. https://doi.org/10.1016/j.cell.2017.08.002.
3. Macrae, T.A., Fothergill-Robinson, J., and Ramalho-Santos, M. (2023). Regulation, functions and transmission of bivalent chromatin during mammalian development. Nat. Rev. Mol. Cell Biol. *24*, 6–26. https://doi.org/10.1038/s41580-022-00518-2.
4. Hanson, R.D., Hess, J.L., Yu, B.D., Ernst, P., van Lohuizen, M., Berns, A., van der Lugt, N.M., Shashikant, C.S., Ruddle, F.H., Seto, M., et al. (1999). Mammalian Trithorax and polycomb-group homologues are antagonistic regulators of homeotic development. Proc. Natl. Acad. Sci. USA *96*, 14372–14377. https://doi.org/10.1073/pnas.96.25.14372.
5. Bernstein, B.E., Mikkelsen, T.S., Xie, X., Kamal, M., Huebert, D.J., Cuff, J., Fry, B., Meissner, A., Wernig, M., Plath, K., et al. (2006). A bivalent chromatin structure marks key developmental genes in embryonic stem cells. Cell *125*, 315–326. https://doi.org/10.1016/j.cell.2006.02.041.
6. Mas, G., Blanco, E., Ballaré, C., Sansó, M., Spill, Y.G., Hu, D., Aoi, Y., Le Dily, F., Shilatifard, A., Marti-Renom, M.A., et al. (2018). Promoter bivalency favors an open chromatin architecture in embryonic stem cells. Nat. Genet. *50*, 1452–1462. https://doi.org/10.1038/s41588-018-0218-5.
7. Douillet, D., Sze, C.C., Ryan, C., Piunti, A., Shah, A.P., Ugarenko, M., Marshall, S.A., Rendleman, E.J., Zha, D., Helmin, K.A., et al. (2020). Uncoupling histone H3K4 trimethylation from developmental gene expression via an equilibrium of COMPASS, Polycomb and DNA methylation. Nat. Genet. *52*, 615–625. https://doi.org/10.1038/s41588-020-0618-1.
8. Hanna, C.W., Taudt, A., Huang, J., Gahurova, L., Kranz, A., Andrews, S., Dean, W., Stewart, A.F., Colomé-Tatché, M., and Kelsey, G. (2018). MLL2 conveys transcription-independent H3K4 trimethylation in oocytes. Nat. Struct. Mol. Biol. *25*, 73–82. https://doi.org/10.1038/s41594-017-0013-5.
9. Hu, M., Yeh, Y.H., Maezawa, S., Nakagawa, T., Yoshida, S., and Namekawa, S.H. (2024). PRC1 directs PRC2-H3K27me3 deposition to shield adult spermatogonial stem cells from differentiation. Nucleic Acids Res. *52*, 2306–2322. https://doi.org/10.1093/nar/gkad1203.
10. Liu, X., Wang, C., Liu, W., Li, J., Li, C., Kou, X., Chen, J., Zhao, Y., Gao, H., Wang, H., et al. (2016). Distinct features of H3K4me3 and H3K27me3 chromatin domains in pre-implantation embryos. Nature *537*, 558–562. https://doi.org/10.1038/nature19362.
11. Lu, X., Zhang, Y., Wang, L., Wang, L., Wang, H., Xu, Q., Xiang, Y., Chen, C., Kong, F., Xia, W., et al. (2021). Evolutionary epigenomic analyses in mammalian early embryos reveal species-specific innovations and conserved principles of imprinting. Sci. Adv. *7*, eabi6178. https://doi.org/10.1126/sciadv.abi6178.
12. Xiang, Y., Zhang, Y., Xu, Q., Zhou, C., Liu, B., Du, Z., Zhang, K., Zhang, B., Wang, X., Gayen, S., et al. (2020). Epigenomic analysis of gastrulation identifies a unique chromatin state for primed pluripotency. Nat. Genet. *52*, 95–105. https://doi.org/10.1038/s41588-019-0545-1.
13. Zheng, H., Huang, B., Zhang, B., Xiang, Y., Du, Z., Xu, Q., Li, Y., Wang, Q., Ma, J., Peng, X., et al. (2016). Resetting Epigenetic Memory by Reprogramming of Histone Modifications in Mammals. Mol. Cell *63*, 1066–1079. https://doi.org/10.1016/j.molcel.2016.08.032.
14. Erkek, S., Hisano, M., Liang, C.Y., Gill, M., Murr, R., Dieker, J., Schübeler, D., van der Vlag, J., Stadler, M.B., and Peters, A.H.F.M. (2013). Molecular determinants of nucleosome retention at CpG-rich sequences in mouse spermatozoa. Nat. Struct. Mol. Biol. *20*, 868–875. https://doi.org/10.1038/nsmb.2599.
15. Hammoud, S.S., Nix, D.A., Zhang, H., Purwar, J., Carrell, D.T., and Cairns, B.R. (2009). Distinctive chromatin in human sperm packages genes for embryo development. Nature *460*, 473–478. https://doi.org/10.1038/nature08162.
16. Rugg-Gunn, P.J., Cox, B.J., Ralston, A., and Rossant, J. (2010). Distinct histone modifications in stem cell lines and tissue lineages from the early mouse embryo. Proc. Natl. Acad. Sci. USA *107*, 10783–10790. https://doi.org/10.1073/pnas.0914507107.
17. Alder, O., Lavial, F., Helness, A., Brookes, E., Pinho, S., Chandrashekran, A., Arnaud, P., Pombo, A., O'Neill, L., and Azuara, V. (2010). Ring1B and Suv39h1 delineate distinct chromatin states at bivalent genes during early mouse lineage commitment. Development *137*, 2483–2492. https://doi.org/10.1242/dev.048363.
18. Mei, H., Kozuka, C., Hayashi, R., Kumon, M., Koseki, H., and Inoue, A. (2021). H2AK119ub1 guides maternal inheritance and zygotic deposition of H3K27me3 in mouse embryos. Nat. Genet. *53*, 539–550. https://doi.org/10.1038/s41588-021-00820-3.
19. Inoue, A., Jiang, L., Lu, F., Suzuki, T., and Zhang, Y. (2017). Maternal H3K27me3 controls DNA methylation-independent imprinting. Nature *547*, 419–424. https://doi.org/10.1038/nature23262.

20. Inoue, A., Jiang, L., Lu, F., and Zhang, Y. (2017). Genomic imprinting of Xist by maternal H3K27me3. Genes Dev. *31*, 1927–1932. https://doi.org/10.1101/gad.304113.117.

21. Inoue, A., Chen, Z., Yin, Q., and Zhang, Y. (2018). Maternal Eed knockout causes loss of H3K27me3 imprinting and random X inactivation in the extraembryonic cells. Genes Dev. *32*, 1525–1536. https://doi.org/10.1101/gad.318675.118.

22. Matoba, S., Kozuka, C., Miura, K., Inoue, K., Kumon, M., Hayashi, R., Ohhata, T., Ogura, A., and Inoue, A. (2022). Noncanonical imprinting sustains embryonic development and restrains placental overgrowth. Genes Dev. *36*, 483–494. https://doi.org/10.1101/gad.349390.122.

23. Zhao, Y., Bai, D., Wu, Y., Zhang, D., Liu, M., Tian, Y., Lu, J., Wang, H., Gao, S., and Lu, Z. (2022). Maternal Ezh1/2 deficiency in oocyte delays H3K27me2/3 restoration and impairs epiblast development responsible for embryonic sub-lethality in mouse. Development *149*, dev200316. https://doi.org/10.1242/dev.200316.

24. Gao, Z., Zhang, J., Bonasio, R., Strino, F., Sawai, A., Parisi, F., Kluger, Y., and Reinberg, D. (2012). PCGF Homologs, CBX Proteins, and RYBP Define Functionally Distinct PRC1 Family Complexes. Mol. Cell *45*, 344–356. https://doi.org/10.1016/j.molcel.2012.01.002.

25. Blackledge, N.P., and Klose, R.J. (2021). The molecular principles of gene regulation by Polycomb repressive complexes. Nat. Rev. Mol. Cell Biol. *22*, 815–833. https://doi.org/10.1038/s41580-021-00398-y.

26. Kim, J.J., and Kingston, R.E. (2022). Context-specific Polycomb mechanisms in development. Nat. Rev. Genet. *23*, 680–695. https://doi.org/10.1038/s41576-022-00499-0.

27. Blackledge, N.P., Farcas, A.M., Kondo, T., King, H.W., McGouran, J.F., Hanssen, L.L.P., Ito, S., Cooper, S., Kondo, K., Koseki, Y., et al. (2014). Variant PRC1 Complex-Dependent H2A Ubiquitylation Drives PRC2 Recruitment and Polycomb Domain Formation. Cell *157*, 1445–1459. https://doi.org/10.1016/j.cell.2014.05.004.

28. Fursova, N.A., Blackledge, N.P., Nakayama, M., Ito, S., Koseki, Y., Farcas, A.M., King, H.W., Koseki, H., and Klose, R.J. (2019). Synergy between Variant PRC1 Complexes Defines Polycomb-Mediated Gene Repression. Mol. Cell *74*, 1020–1036.e8. https://doi.org/10.1016/j.molcel.2019.03.024.

29. Isono, K., Endo, T.A., Ku, M., Yamada, D., Suzuki, R., Sharif, J., Ishikura, T., Toyoda, T., Bernstein, B.E., and Koseki, H. (2013). SAM domain polymerization links subnuclear clustering of PRC1 to gene silencing. Dev. Cell *26*, 565–577. https://doi.org/10.1016/j.devcel.2013.08.016.

30. Blackledge, N.P., Fursova, N.A., Kelley, J.R., Huseyin, M.K., Feldmann, A., and Klose, R.J. (2020). PRC1 Catalytic Activity Is Central to Polycomb System Function. Mol. Cell *77*, 857–874.e9. https://doi.org/10.1016/j.molcel.2019.12.001.

31. Tamburri, S., Lavarone, E., Fernández-Pérez, D., Conway, E., Zanotti, M., Manganaro, D., and Pasini, D. (2020). Histone H2AK119 Mono-Ubiquitination Is Essential for Polycomb-Mediated Transcriptional Repression. Mol. Cell *77*, 840–856.e5. https://doi.org/10.1016/j.molcel.2019.11.021.

32. Sijm, A., Atlasi, Y., van der Knaap, J.A., Wolf van der Meer, J., Chalkley, G.E., Bezstarosti, K., Dekkers, D.H.W., Doff, W.A.S., Ozgur, Z., van IJcken, W.F.J., et al. (2022). USP7 regulates the ncPRC1 Polycomb axis to stimulate genomic H2AK119ub1 deposition uncoupled from H3K27me3. Sci. Adv. *8*, eabq7598. https://doi.org/10.1126/sciadv.abq7598.

33. Matsuwaka, M., Kumon, M., and Inoue, A. (2025). H3K27 dimethylation dynamics reveal stepwise establishment of facultative heterochromatin in early mouse embryos. Nat. Cell Biol. *27*, 28–38. https://doi.org/10.1038/s41556-024-01553-1.

34. Hickey, G.J., Wike, C.L., Nie, X., Guo, Y., Tan, M., Murphy, P.J., and Cairns, B.R. (2022). Establishment of developmental gene silencing by ordered polycomb complex recruitment in early zebrafish embryos. eLife *11*, e67738. https://doi.org/10.7554/eLife.67738.

35. Sugishita, H., Kondo, T., Ito, S., Nakayama, M., Yakushiji-Kaminatsui, N., Kawakami, E., Koseki, Y., Ohinata, Y., Sharif, J., Harachi, M., et al. (2021). Variant PCGF1-PRC1 links PRC2 recruitment with differentiation-associated transcriptional inactivation at target genes. Nat. Commun. *12*, 5341. https://doi.org/10.1038/s41467-021-24894-z.

36. Petracovici, A., and Bonasio, R. (2021). Distinct PRC2 subunits regulate maintenance and establishment of Polycomb repression during differentiation. Mol. Cell *81*, 2625–2639.e5. https://doi.org/10.1016/j.molcel.2021.03.038.

37. Healy, E., Mucha, M., Glancy, E., Fitzpatrick, D.J., Conway, E., Neikes, H.K., Monger, C., Van Mierlo, G., Baltissen, M.P., Koseki, Y., et al. (2019). PRC2.1 and PRC2.2 Synergize to Coordinate H3K27 Trimethylation. Mol. Cell *76*, 437–452.e6. https://doi.org/10.1016/j.molcel.2019.08.012.

38. Højfeldt, J.W., Hedehus, L., Laugesen, A., Tatar, T., Wiehle, L., and Helin, K. (2019). Non-core Subunits of the PRC2 Complex Are Collectively Required for Its Target-Site Specificity. Mol. Cell *76*, 423–436.e3. https://doi.org/10.1016/j.molcel.2019.07.031.

39. Pengelly, A.R., Kalb, R., Finkl, K., and Müller, J. (2015). Transcriptional repression by PRC1 in the absence of H2A monoubiquitylation. Genes Dev. *29*, 1487–1492. https://doi.org/10.1101/gad.265439.115.

40. Illingworth, R.S., Moffat, M., Mann, A.R., Read, D., Hunter, C.J., Pradeepa, M.M., Adams, I.R., and Bickmore, W.A. (2015). The E3 ubiquitin ligase activity of RING1B is not essential for early mouse development. Genes Dev. *29*, 1897–1902. https://doi.org/10.1101/gad.268151.115.

41. Ernst, J., and Kellis, M. (2012). ChromHMM: automating chromatin-state discovery and characterization. Nat. Methods *9*, 215–216. https://doi.org/10.1038/nmeth.1906.

42. Du, Z., Zheng, H., Kawamura, Y.K., Zhang, K., Gassler, J., Powell, S., Xu, Q., Lin, Z., Xu, K., Zhou, Q., et al. (2020). Polycomb Group Proteins Regulate Chromatin Architecture in Mouse Oocytes and Early Embryos. Mol. Cell *77*, 825–839.e7. https://doi.org/10.1016/j.molcel.2019.11.011.

43. de Vries, W.N., Binns, L.T., Fancher, K.S., Dean, J., Moore, R., Kemler, R., and Knowles, B.B. (2000). Expression of Cre recombinase in mouse oocytes: a means to study maternal effect genes. Genesis *26*, 110–112. https://doi.org/10.1002/(SICI)1526-968X(200002)26:2<110::AID-GENE2>3.0.CO;2-8.

44. Andreu-Vieyra, C.V., Chen, R., Agno, J.E., Glaser, S., Anastassiadis, K., Stewart, A.F., and Matzuk, M.M. (2010). MLL2 is required in oocytes for bulk histone 3 lysine 4 trimethylation and transcriptional silencing. PLoS Biol. *8*, e1000453. https://doi.org/10.1371/journal.pbio.1000453.

45. Zhu, Y.Z., Yu, J.L., Rong, Y., Wu, Y.W., Li, Y., Zhang, L.J., Pan, Y.H., Fan, H.Y., and Shen, L. (2021). Genomewide decoupling of H2AK119ub1 and H3K27me3 in early mouse development. Sci. Bull. *66*, 2489–2497. https://doi.org/10.1016/j.scib.2021.06.010.

46. Hanna, C.W., Huang, J., Belton, C., Reinhardt, S., Dahl, A., Andrews, S., Stewart, A.F., Kranz, A., and Kelsey, G. (2022). Loss of histone methyltransferase SETD1B in oogenesis results in the redistribution of genomic histone 3 lysine 4 trimethylation. Nucleic Acids Res. *50*, 1993–2004. https://doi.org/10.1093/nar/gkac051.

47. Sha, Q.Q., Zhu, Y.Z., Xiang, Y., Yu, J.L., Fan, X.Y., Li, Y.C., Wu, Y.W., Shen, L., and Fan, H.Y. (2021). Role of CxxC-finger protein 1 in establishing mouse oocyte epigenetic landscapes. Nucleic Acids Res. *49*, 2569–2582. https://doi.org/10.1093/nar/gkab107.

48. Yuan, W., Xu, M., Huang, C., Liu, N., Chen, S., and Zhu, B. (2011). H3K36 Methylation Antagonizes PRC2-mediated H3K27 Methylation. J. Biol. Chem. *286*, 7983–7989. https://doi.org/10.1074/jbc.M110.194027.

49. Schmitges, F.W., Prusty, A.B., Faty, M., Stützer, A., Lingaraju, G.M., Aiwazian, J., Sack, R., Hess, D., Li, L., Zhou, S., et al. (2011). Histone methylation by PRC2 is inhibited by active chromatin marks. Mol. Cell *42*, 330–341. https://doi.org/10.1016/j.molcel.2011.03.025.

50. Voigt, P., LeRoy, G., Drury, W.J., 3rd, Zee, B.M., Son, J., Beck, D.B., Young, N.L., Garcia, B.A., and Reinberg, D. (2012). Asymmetrically modified nucleosomes. Cell *151*, 181–193. https://doi.org/10.1016/j.cell.2012.09.002.

51. Xu, Q., Xiang, Y., Wang, Q., Wang, L., Brind'Amour, J., Bogutz, A.B., Zhang, Y., Zhang, B., Yu, G., Xia, W., et al. (2019). SETD2 regulates the maternal epigenome, genomic imprinting and embryonic development. Nat. Genet. *51*, 844–856. https://doi.org/10.1038/s41588-019-0398-7.

52. Shirane, K., Miura, F., Ito, T., and Lorincz, M.C. (2020). NSD1-deposited H3K36me2 directs de novo methylation in the mouse male germline and counteracts Polycomb-associated silencing. Nat. Genet. *52*, 1088–1098. https://doi.org/10.1038/s41588-020-0689-z.

53. Streubel, G., Watson, A., Jammula, S.G., Scelfo, A., Fitzpatrick, D.J., Oliviero, G., McCole, R., Conway, E., Glancy, E., Negri, G.L., et al. (2018). The H3K36me2 Methyltransferase Nsd1 Demarcates PRC2-Mediated H3K27me2 and H3K27me3 Domains in Embryonic Stem Cells. Mol. Cell *70*, 371–379.e5. https://doi.org/10.1016/j.molcel.2018.02.027.

54. Lu, X., Wang, L., Liu, B., Hu, X., Wang, Z., Liu, L., Yu, G., Dong, L., Kong, F., Fan, Q., et al. (2025). Reprogramming of H3K36me2 guides lineage-specific post-implantation de novo DNA methylation. Nat. Cell Biol. *27*, 2128–2142. https://doi.org/10.1038/s41556-025-01805-8.

55. Kawamura, Y.K., Ozonov, E.A., Papasaikas, P., Kondo, T., Nguyen, N.V., Stadler, M.B., Smallwood, S.A., Koseki, H., and Peters, A.H.F.M. (2025). Preventing CpG hypermethylation in oocytes safeguards mouse development. Dev. Cell *60*, 3285–3303.e9. https://doi.org/10.1016/j.devcel.2025.08.005.

56. Yano, S., Ishiuchi, T., Abe, S., Namekawa, S.H., Huang, G., Ogawa, Y., and Sasaki, H. (2022). Histone H3K36me2 and H3K36me3 form a chromatin platform essential for DNMT3A-dependent DNA methylation in mouse oocytes. Nat. Commun. *13*, 4440. https://doi.org/10.1038/s41467-022-32141-2.

57. Inoue, A. (2023). Noncanonical imprinting: intergenerational epigenetic inheritance mediated by Polycomb complexes. Curr. Opin. Genet. Dev. *78*, 102015. https://doi.org/10.1016/j.gde.2022.102015.

58. Inoue, K., Hirose, M., Inoue, H., Hatanaka, Y., Honda, A., Hasegawa, A., Mochida, K., and Ogura, A. (2017). The Rodent-Specific MicroRNA Cluster within the Sfmbt2 Gene Is Imprinted and Essential for Placental Development. Cell Rep. *19*, 949–956. https://doi.org/10.1016/j.celrep.2017.04.018.

59. Inoue, K., Ogonuki, N., Kamimura, S., Inoue, H., Matoba, S., Hirose, M., Honda, A., Miura, K., Hada, M., Hasegawa, A., et al. (2020). Loss of H3K27me3 imprinting in the Sfmbt2 miRNA cluster causes enlargement of cloned mouse placentas. Nat. Commun. *11*, 2150. https://doi.org/10.1038/s41467-020-16044-8.

60. Posfai, E., Kunzmann, R., Brochard, V., Salvaing, J., Cabuy, E., Roloff, T.C., Liu, Z.C., Tardat, M., van Lohuizen, M., Vidal, M., et al. (2012). Polycomb function during oogenesis is required for mouse embryonic development. Genes Dev. *26*, 920–932. https://doi.org/10.1101/gad.188094.112.

61. Finogenova, K., Bonnet, J., Poepsel, S., Schäfer, I.B., Finkl, K., Schmid, K., Litz, C., Strauss, M., Benda, C., and Müller, J. (2020). Structural basis for PRC2 decoding of active histone methylation marks H3K36me2/3. eLife *9*, e61964. https://doi.org/10.7554/eLife.61964.

62. Mendenhall, E.M., Koche, R.P., Truong, T., Zhou, V.W., Issac, B., Chi, A.S., Ku, M., and Bernstein, B.E. (2010). GC-rich sequence elements recruit PRC2 in mammalian ES cells. PLoS Genet. *6*, e1001244. https://doi.org/10.1371/journal.pgen.1001244.

63. Lynch, M.D., Smith, A.J.H., De Gobbi, M., Flenley, M., Hughes, J.R., Vernimmen, D., Ayyub, H., Sharpe, J.A., Sloane-Stanley, J.A., Sutherland, L., et al. (2011). An interspecies analysis reveals a key role for unmethylated CpG dinucleotides in vertebrate Polycomb complex recruitment. EMBO J. *31*, 317–329. https://doi.org/10.1038/emboj.2011.399.

64. Riising, E.M., Comet, I., Leblanc, B., Wu, X., Johansen, J.V., and Helin, K. (2014). Gene silencing triggers polycomb repressive complex 2 recruitment to CpG islands genome wide. Mol. Cell *55*, 347–360. https://doi.org/10.1016/j.molcel.2014.06.005.

65. Hosogane, M., Funayama, R., Shirota, M., and Nakayama, K. (2016). Lack of Transcription Triggers H3K27me3 Accumulation in the Gene Body. Cell Rep. *16*, 696–706. https://doi.org/10.1016/j.celrep.2016.06.034.

66. Mikkelsen, T.S., Hanna, J., Zhang, X., Ku, M., Wernig, M., Schorderet, P., Bernstein, B.E., Jaenisch, R., Lander, E.S., and Meissner, A. (2008). Dissecting direct reprogramming through integrative genomic analysis. Nature *454*, 49–55. https://doi.org/10.1038/nature07056.

67. Jadhav, U., Nalapareddy, K., Saxena, M., O'Neill, N.K., Pinello, L., Yuan, G.C., Orkin, S.H., and Shivdasani, R.A. (2016). Acquired Tissue-Specific Promoter Bivalency Is a Basis for PRC2 Necessity in Adult Cells. Cell *165*, 1389–1400. https://doi.org/10.1016/j.cell.2016.04.031.

68. Voigt, P., Tee, W.W., and Reinberg, D. (2013). A double take on bivalent promoters. Genes Dev. *27*, 1318–1338. https://doi.org/10.1101/gad.219626.113.

69. Mikkelsen, T.S., Ku, M., Jaffe, D.B., Issac, B., Lieberman, E., Giannoukos, G., Alvarez, P., Brockman, W., Kim, T.K., Koche, R.P., et al. (2007). Genome-wide maps of chromatin state in pluripotent and lineage-committed cells. Nature *448*, 553–560. https://doi.org/10.1038/nature06008.

70. Szczurek, A.T., Dimitrova, E., Kelley, J.R., Blackledge, N.P., and Klose, R.J. (2024). The Polycomb system sustains promoters in a deep OFF state by limiting pre-initiation complex formation to counteract transcription. Nat. Cell Biol. *26*, 1700–1711. https://doi.org/10.1038/s41556-024-01493-w.

71. Dobrinić, P., Szczurek, A.T., and Klose, R.J. (2021). PRC1 drives Polycomb-mediated gene repression by controlling transcription initiation and burst frequency. Nat. Struct. Mol. Biol. *28*, 811–824. https://doi.org/10.1038/s41594-021-00661-y.

72. Lauberth, S.M., Nakayama, T., Wu, X., Ferris, A.L., Tang, Z., Hughes, S.H., and Roeder, R.G. (2013). H3K4me3 interactions with TAF3 regulate preinitiation complex assembly and selective gene activation. Cell *152*, 1021–1036. https://doi.org/10.1016/j.cell.2013.01.052.

73. Cookis, T., Lydecker, A., Sauer, P., Kasinath, V., and Nogales, E. (2024). Structural basis for the inhibition of PRC2 by active transcription histone posttranslational modifications. Nat. Struct. Mol. Biol. *32*, 393–404. https://doi.org/10.1101/2024.02.09.579730.

74. Holoch, D., Wassef, M., Lövkvist, C., Zielinski, D., Aflaki, S., Lombard, B., Héry, T., Loew, D., Howard, M., and Margueron, R. (2021). A cis-acting mechanism mediates transcriptional memory at Polycomb target genes in mammals. Nat. Genet. *53*, 1686–1697. https://doi.org/10.1038/s41588-021-00964-2.

75. Chen, S., Ma, J., Wu, F., Xiong, L.J., Ma, H., Xu, W., Lv, R., Li, X., Villen, J., Gygi, S.P., et al. (2012). The histone H3 Lys 27 demethylase JMJD3 regulates gene expression by impacting transcriptional elongation. Genes Dev. *26*, 1364–1375. https://doi.org/10.1101/gad.186056.111.

76. Policarpi, C., Munafò, M., Tsagkris, S., Carlini, V., and Hackett, J.A. (2024). Systematic epigenome editing captures the context-dependent instructive function of chromatin modifications. Nat. Genet. *56*, 1168–1180. https://doi.org/10.1038/s41588-024-01706-w.

77. Wang, H., Fan, Z., Shliaha, P.V., Miele, M., Hendrickson, R.C., Jiang, X., and Helin, K. (2023). H3K4me3 regulates RNA polymerase II promoter-proximal pause-release. Nature *615*, 339–348. https://doi.org/10.1038/s41586-023-05780-8.

78. Wang, H., and Helin, K. (2024). Roles of H3K4 methylation in biology and disease. Trends Cell Biol. *35*, 115–128. https://doi.org/10.1016/j.tcb.2024.06.001.

79. Estarás, C., Fueyo, R., Akizu, N., Beltrán, S., and Martínez-Balbás, M.A. (2013). RNA polymerase II progression through H3K27me3-enriched

gene bodies requires JMJD3 histone demethylase. Mol. Biol. Cell *24*, 351–360. https://doi.org/10.1091/mbc.e12-07-0561.

80. Xiong, Z., Xu, K., Lin, Z., Kong, F., Wang, Q., Quan, Y., Sha, Q.Q., Li, F., Zou, Z., Liu, L., et al. (2022). Ultrasensitive Ribo-seq reveals translational landscapes during mammalian oocyte-to-embryo transition and pre-implantation development. Nat. Cell Biol. *24*, 968–980. https://doi.org/10.1038/s41556-022-00928-6.

81. Stock, J.K., Giadrossi, S., Casanova, M., Brookes, E., Vidal, M., Koseki, H., Brockdorff, N., Fisher, A.G., and Pombo, A. (2007). Ring1-mediated ubiquitination of H2A restrains poised RNA polymerase II at bivalent genes in mouse ES cells. Nat. Cell Biol. *9*, 1428–1435. https://doi.org/10.1038/ncb1663.

82. Akasaka, T., van Lohuizen, M., van der Lugt, N., Mizutani-Koseki, Y., Kanno, M., Taniguchi, M., Vidal, M., Alkema, M., Berns, A., and Koseki, H. (2001). Mice doubly deficient for the Polycomb Group genes Mel18 and Bmi1 reveal synergy and requirement for maintenance but not initiation of Hox gene expression. Development *128*, 1587–1597. https://doi.org/10.1242/dev.128.9.1587.

83. Scelfo, A., Fernández-Pérez, D., Tamburri, S., Zanotti, M., Lavarone, E., Soldi, M., Bonaldi, T., Ferrari, K.J., and Pasini, D. (2019). Functional Landscape of PCGF Proteins Reveals Both RING1A/B-Dependent-And RING1A/B-Independent-Specific Activities. Mol. Cell *74*, 1037–1052.e7. https://doi.org/10.1016/j.molcel.2019.04.002.

84. Hoffmann, J., Schütze, T.M., Kolodziejczyk, A., Küster, K., Kränkel, A., Reinhardt, S., Derihaci, R.P., Birdir, C., Wimberger, P., Koseki, H., et al. (2025). Canonical and non-canonical PRC1 differentially contribute to regulation of neural stem cell fate. Life Sci. Alliance *8*, e202403006. https://doi.org/10.26508/lsa.202403006.

85. Huseyin, M.K., and Klose, R.J. (2021). Live-cell single particle tracking of PRC1 reveals a highly dynamic system with low target site occupancy. Nat. Commun. *12*, 887. https://doi.org/10.1038/s41467-021-21130-6.

86. Chen, Z., Yin, Q., Inoue, A., Zhang, C., and Zhang, Y. (2019). Allelic H3K27me3 to allelic DNA methylation switch maintains noncanonical imprinting in extraembryonic cells. Sci. Adv. *5*, eaay7246. https://doi.org/10.1126/sciadv.aay7246.

87. Liu, B., Xu, Q., Wang, Q., Feng, S., Lai, F., Wang, P., Zheng, F., Xiang, Y., Wu, J., Nie, J., et al. (2020). The landscape of RNA Pol II binding reveals a stepwise transition during ZGA. Nature *587*, 139–144. https://doi.org/10.1038/s41586-020-2847-y.

88. Sakamoto, M., Ito, A., Wakayama, S., Sasaki, H., Wakayama, T., and Ishiuchi, T. (2024). Detection of newly synthesized RNA reveals transcriptional reprogramming during ZGA and a role of Obox3 in totipotency acquisition. Cell Rep. *43*, 114118. https://doi.org/10.1016/j.celrep.2024.114118.

89. Chen, Z., Djekidel, M.N., and Zhang, Y. (2021). Distinct dynamics and functions of H2AK119ub1 and H3K27me3 in mouse preimplantation embryos. Nat. Genet. *53*, 551–563. https://doi.org/10.1038/s41588-021-00821-2.

90. Inoue, A., Sunaga, K., Aoki, F., and Zhang, Y. (2014). siRNA-mediated depletion of stable proteins in mouse oocytes. Protocols Exchange. https://doi.org/10.1038/protex.2014.024.

91. Wan, C., Mahara, S., Sun, C., Doan, A., Chua, H.K., Xu, D., Bian, J., Li, Y., Zhu, D., Sooraj, D., et al. (2021). Genome-scale CRISPR-Cas9 screen of Wnt/β-catenin signaling identifies therapeutic targets for colorectal cancer. Sci. Adv. *7*, eabf2567. https://doi.org/10.1126/sciadv.abf2567.

92. Peeters, J.G.C., Picavet, L.W., Coenen, S.G.J.M., Mauthe, M., Vervoort, S.J., Mocholi, E., de Heus, C., Klumperman, J., Vastert, S.J., Reggiori, F., et al. (2019). Transcriptional and epigenetic profiling of nutrient-deprived cells to identify novel regulators of autophagy. Autophagy *15*, 98–112. https://doi.org/10.1080/15548627.2018.1509608.

93. del Mar Lorente, M., Marcos-Gutiérrez, C., Pérez, C., Schoorlemmer, J., Ramírez, A., Magin, T., and Vidal, M. (2000). Loss- and gain-of-function mutations show a polycomb group function for Ring1A in mice. Development *127*, 5093–5100. https://doi.org/10.1242/dev.127.23.5093.

94. Langmead, B., and Salzberg, S.L. (2012). Fast gapped-read alignment with Bowtie 2. Nat. Methods *9*, 357–359. https://doi.org/10.1038/nmeth.1923.

95. Tarasov, A., Vilella, A.J., Cuppen, E., Nijman, I.J., and Prins, P. (2015). Sambamba: fast processing of NGS alignment formats. Bioinformatics *31*, 2032–2034. https://doi.org/10.1093/bioinformatics/btv098.

96. Li, H., Handsaker, B., Wysoker, A., Fennell, T., Ruan, J., Homer, N., Marth, G., Abecasis, G., and Durbin, R.; 1000 Genome Project Data Processing Subgroup (2009). The Sequence Alignment/Map format and SAMtools. Bioinformatics *25*, 2078–2079. https://doi.org/10.1093/bioinformatics/btp352.

97. Robinson, J.T., Thorvaldsdóttir, H., Winckler, W., Guttman, M., Lander, E.S., Getz, G., and Mesirov, J.P. (2011). Integrative genomics viewer. Nat. Biotechnol. *29*, 24–26. https://doi.org/10.1038/nbt.1754.

98. Ramírez, F., Dündar, F., Diehl, S., Grüning, B.A., and Manke, T. (2014). deepTools: a flexible platform for exploring deep-sequencing data. Nucleic Acids Res. *42*, W187–W191. https://doi.org/10.1093/nar/gku365.

99. Dobin, A., Davis, C.A., Schlesinger, F., Drenkow, J., Zaleski, C., Jha, S., Batut, P., Chaisson, M., and Gingeras, T.R. (2013). STAR: ultrafast universal RNA-seq aligner. Bioinformatics *29*, 15–21. https://doi.org/10.1093/bioinformatics/bts635.

100. Liao, Y., Smyth, G.K., and Shi, W. (2014). featureCounts: an efficient general purpose program for assigning sequence reads to genomic features. Bioinformatics *30*, 923–930. https://doi.org/10.1093/bioinformatics/btt656.

101. Li, B., and Dewey, C.N. (2011). RSEM: accurate transcript quantification from RNA-Seq data with or without a reference genome. BMC Bioinform. *12*, 323. https://doi.org/10.1186/1471-2105-12-323.

102. Robinson, M.D., McCarthy, D.J., and Smyth, G.K. (2010). edgeR: a Bioconductor package for differential expression analysis of digital gene expression data. Bioinformatics *26*, 139–140. https://doi.org/10.1093/bioinformatics/btp616.

103. Krueger, F., and Andrews, S. (2016). SNPsplit: Allele-specific splitting of alignments between genomes with known SNP genotypes. F1000Res. *5*, 1479.

104. Zhang, Y., Liu, T., Meyer, C.A., Eeckhoute, J., Johnson, D.S., Bernstein, B.E., Nusbaum, C., Myers, R.M., Brown, M., Li, W., et al. (2008). Model-based Analysis of ChIP-Seq (MACS). Genome Biol. *9*, R137. https://doi.org/10.1186/gb-2008-9-9-r137.

105. Quinlan, A.R., and Hall, I.M. (2010). BEDTools: a flexible suite of utilities for comparing genomic features. Bioinformatics *26*, 841–842. https://doi.org/10.1093/bioinformatics/btq033.

106. Heinz, S., Benner, C., Spann, N., Bertolino, E., Lin, Y.C., Laslo, P., Cheng, J.X., Murre, C., Singh, H., and Glass, C.K. (2010). Simple Combinations of Lineage-Determining Transcription Factors Prime Cis-regulatory Elements Required for Macrophage and B Cell Identities. Mol. Cell *38*, 576–589. https://doi.org/10.1016/j.molcel.2010.05.004.

107. Zhou, Y.Y., Zhou, B., Pache, L., Chang, M., Khodabakhshi, A.H., Tanaseichuk, O., Benner, C., and Chanda, S.K. (2019). Metascape provides a biologist-oriented resource for the analysis of systems-level datasets. Nat. Commun. *10*, 1523. https://doi.org/10.1038/s41467-019-09234-6.

108. Takada, T., Ebata, T., Noguchi, H., Keane, T.M., Adams, D.J., Narita, T., Shin-I, T., Fujisawa, H., Toyoda, A., Abe, K., et al. (2013). The ancestor of extant Japanese fancy mice contributed to the mosaic genomes of classical inbred strains. Genome Res. *23*, 1329–1338. https://doi.org/10.1101/gr.156497.113.

109. Glaser, S., Schaft, J., Lubitz, S., Vintersten, K., van der Hoeven, F., Tufteland, K.R., Aasland, R., Anastassiadis, K., Ang, S.L., and Stewart, A.F. (2006). Multiple epigenetic maintenance factors implicated by the

loss of Mll2 in mouse development. Development *133*, 1423–1432. https://doi.org/10.1242/dev.02302.

110. Concordet, J.P., and Haeussler, M. (2018). CRISPOR: intuitive guide selection for CRISPR/Cas9 genome editing experiments and screens. Nucleic Acids Res. *46*, W242–W245. https://doi.org/10.1093/nar/gky354.
111. Gu, B., Pósfai, E., and Rossant, J. (2018). Efficient generation of targeted large insertions by microinjection into two-cell-stage mouse embryos. Nat. Biotechnol. *36*, 632–637. https://doi.org/10.1038/nbt.4166.
112. Inoue, A., Akiyama, T., Nagata, M., and Aoki, F. (2007). The perivitelline space-forming capacity of mouse oocytes is associated with meiotic competence. J. Reprod. Dev. *53*, 1043–1052. https://doi.org/10.1262/jrd.19064.
113. Brind'Amour, J., Liu, S., Hudson, M., Chen, C., Karimi, M.M., and Lorincz, M.C. (2015). An ultra-low-input native ChIP-seq protocol for genome-wide profiling of rare cell populations. Nat. Commun. *6*, 6033. https://doi.org/10.1038/ncomms7033.
114. Kaya-Okur, H.S., Janssens, D.H., Henikoff, J.G., Ahmad, K., and Henikoff, S. (2020). Efficient low-cost chromatin profiling with CUT&Tag. Nat. Protoc. *15*, 3264–3283. https://doi.org/10.1038/s41596-020-0373-x.
115. Hayashi, R., and Inoue, A. (2023). Low-Input CUT&RUN for Mouse Oocytes and Preimplantation Embryos. Methods Mol. Biol. *2577*, 83–92. https://doi.org/10.1007/978-1-0716-2724-2_6.
116. Skene, P.J., and Henikoff, S. (2017). An efficient targeted nuclease strategy for high-resolution mapping of DNA binding sites. eLife *6*, e21856. https://doi.org/10.7554/eLife.21856.
117. Yu, G.C., Wang, L.G., and He, Q.Y. (2015). ChIPseeker: an R/Bioconductor package for ChIP peak annotation, comparison and visualization. Bioinformatics *31*, 2382–2383. https://doi.org/10.1093/bioinformatics/btv145.

Please cite this article in press as: Mei et al., H2AK119ub1-MLL2 counteraction underlies heritable H3K27me3 formation in oocytes, Molecular Cell (2026), https://doi.org/10.1016/j.molcel.2026.03.014

STAR★METHODS

KEY RESOURCES TABLE

REAGENT or RESOURCE	SOURCE	IDENTIFIER
Antibodies		
rabbit polyclonal anti-H3K4me3	Active Motif	39159; RRID:AB_2615077
rabbit polyclonal anti-H3K27me3	Diagenode	C15410069; RRID:AB_2814977
mouse monoclonal anti-H3K36me2	MAB Institute	MABI0332; RRID:AB_2650523
rabbit polyclonal anti-H3K36me3	Active Motif	61022; RRID:AB_2614986
Rabbit monoclonal anti-H2AK119ub1	Cell Signaling Technology	8240; RRID:AB10891618
mouse monoclonal anti-H3K27me3	Active Motif	61017; RRID:AB_2614987
mouse monoclonal anti-H3K4me3	Millipore	05-1339; RRID:AB_10514604
Alexa Flour 488 donkey anti-mouse IgG	Thermo Fisher Scientific	A-21202
Alexa Flour 568 donkey anti-rabbit IgG	Thermo Fisher Scientific	A10042
Chemicals, peptides, and recombinant proteins		
CARD HyperOva	Kyudo	N/A
HEPES-buffered KSOM	Inoue et al.[90]	N/A
Human Tubal Fluid (HTF) medium	Inoue et al.[90]	N/A
3-Isobutyl-1-methylxanthine (IBMX)	Merck	I7018
pregnant mare serum gonadotropin (PMSG)	Aska animal health	N/A
human chorionic gonadotropin (hCG)	Aska animal health	N/A
BSA	Merck	12657
KSOM	Inoue et al.[90]	N/A
M2 medium containing hyaluronidase	Merck Millipore	MR-015-D
α-MEM	Thermo Fisher Scientific	12571-063
Fetal Bovine Serum	Sigma	172012-500ML
Human EGF Recombinant Protein	Thermo Fisher Scientific	PHG0311
cytochalasin B	Merck	C6762
Sendai virus (HVJ)	Cosmo Bio	CF001EX
CARD FERTIUP	Kyudo	N/A
paraformaldehyde (PFA)	Wako	162-16065
Mayer's Hematoxylin Solution	Wako	131-09665
Pure Eosin	Muto Pure Chemicals	32042
0.5%Periodic Acid Solution	Wako	164-19705
PBS	Wako	049-29793
Vectashield anti-fade solution with 4',6-diamidino-2-phenylindole (DAPI)	Vector Laboratories	H-1200
Acid Tyrodes' solution	Merck	MR-004D
Nuclei EZ lysis buffer	Sigma	NUC-101
complete EDTA-free protease inhibitor cocktail	Merck	11836170001
phenylmethanesulfonyl fluoride	Merck	P7626
Triton X-100	Merck	93443
deoxycholate	Nacalai	10712-54
MNase	NEB	M0247S
PEG6000	Hampton Research	HR2-533
DTT	Nacalai	N/A
EDTA	Thermo Fisher Scientific	15575020
Dynabeads Protein A	Thermo Fisher Scientific	10006D

(*Continued on next page*)

Please cite this article in press as: Mei et al., H2AK119ub1-MLL2 counteraction underlies heritable H3K27me3 formation in oocytes, Molecular Cell (2026), https://doi.org/10.1016/j.molcel.2026.03.014

Continued

REAGENT or RESOURCE	SOURCE	IDENTIFIER
Dynabeads Protein G	Thermo Fisher Scientific	10007D
phenol-chloroform-isopropanol	Fujifilm	311-90151
I-SceI	NEB	R0694
Cas9 mRNA	Matsuwaka et al.[33]	N/A
Protein A-MNase	Skene and Henikoff	N/A
Critical commercial assays		
GeneArt Precision gRNA Synthesis Kit	Thermo Fisher	A29377
NEBNext Ultra II DNA Library Prep Kit for Illumina	NEB	E7645
SPRIselect beads	Beckman Coulter	B23318
KAPA Hifi 2X mater PCR mix	KAPA Biosystems	KK2605
NEBNext Multiplex Oligos for Illumina	NEB	E6440
SMART-Seq v4 Ultra Low Input RNA Kit for Sequencing	TAKARA	634890
Nextera XT DNA Library Preparation Kit	Illumina	FC-131-1024
Deposited data		
CATCH-seq and CUT&RUN data	This paper	GEO: GSE292333
RNA-seq data	This paper	GEO: GSE292237
H3K27me3 data in GOs and FGOs	Zheng et al.[13]	GEO: GSE76687
H3K27me3 data in Pcgf1/6 DKO FGOs	Mei et al.[18]	GEO: GSE153496
RNA-seq data in Pcgf1/6 DKO FGOs	Mei et al.[18]	GEO: GSE153496
H2AK119ub1 data in 7d-GOs and FGOs	Mei et al.[18]	GEO: GSE153496
H3K4me3 data in GOs and FGOs	Hanna et al.[8]	GEO: GSE93941
RNA-seq data in Eed KO FGOs	Du et al.[42]	GEO: GSE118263
RNA-seq data in Ring1a/b DKO FGOs	Du et al.[42]	GEO: GSE132156
H2AK119ub1, H3K27me3, and H3K4me3 CUT&Tag data in mouse undifferentiated spermatogonia	Hu et al.[9]	GEO: GSE221942
H2AK119ub1 and H3K27me3 ChIP-seq data in DLD1	Sijm et al.[32]	GEO: GSE193014
H3K4me3 ChIP-seq data in DLD1	Wan et al.[91]	GEO: GSE156081
H2AK119ub1 and H3K27me3 ChIP-seq data in HAP1	Sijm et al.[32]	GEO: GSE193014
H3K4me3 ChIP-seq data in HAP1	Peeters et al.[92]	GEO: GSE107599
Experimental models: Cell lines		
Drosophila melanogaster S2 cells	Thermo Fisher Scientific	R69007
Experimental models: Organisms/strains		
Mouse: *Zp3*^{Cre}/*Pcgf1*$^{fl/fl}$/*Pcgf6*$^{fl/fl}$	Mei et al.[18]	N/A
Mouse: *Zp3*^{Cre}/*Pcgf1*$^{fl/fl}$/*Pcgf6*$^{fl/fl}$/*Mll2*$^{fl/fl}$	This study	N/A
Mouse: *Ring1a*-null	del Mar Lorente et al.[93]	N/A
Mouse: *Zp3*^{Cre}/*Ring1a*$^{-/-}$/*Ring1b*$^{CPM/CPM}$	This study	N/A
Mouse: *Zp3*^{Cre}/*Pcgf1*$^{fl/fl}$/*Pcgf6*$^{fl/fl}$/*C2MC*$^{+/-}$	This study	N/A
Mouse: *Zp3*^{Cre} [C57BL/6-Tg(Zp3-cre)93Knw/J]	Jackson Laboratory	003651
Mouse: JF1/Msf	RIKEN Bioresource Research Center	RBRC00639
Mouse: B6D2F1/Crl	Jackson Laboratory	N/A
Jcl:ICR	CLEA Japan	N/A
Oligonucleotides		
See Table S4 for oligonucleotides	This paper	N/A
I-SceI carrier DNA	Matsuwaka et al.[33]	N/A

(*Continued on next page*)

Please cite this article in press as: Mei et al., H2AK119ub1-MLL2 counteraction underlies heritable H3K27me3 formation in oocytes, Molecular Cell (2026), https://doi.org/10.1016/j.molcel.2026.03.014

Continued

REAGENT or RESOURCE	SOURCE	IDENTIFIER
Software and algorithms		
LASX software	Leica	https://www.leica-microsystems.com/products/microscope-software/p/leica-las-x-ls/?country=JP
TrimGalore(version 0.6.4)	N/A	https://github.com/FelixKrueger/TrimGalore
bowtie2 (version 2.3.5)	Langmead and Salzberg[94]	http://bowtie-bio.sourceforge.net/bowtie2/index.shtml
Sambamba (version 1.0.1)	Tarasov et al.[95]	https://github.com/biod/sambamba
Samtools (version 1.7)	Li et al.[96]	https://www.htslib.org/download/
Integrative Genomics Viewer (version 2.8.0)	Robinson et al.[97]	https://igv.org
deepTools2	Ramirez et al.[98]	https://deeptools.readthedocs.io/en/latest/index.html
chromHMM (version 1.27)	Ernst et al.[41]	https://ernstlab.github.io/ChromHMM/
STAR (version 2.7.6)	Dobin et al.[99]	https://github.com/alexdobin/STAR
featureCounts (version 1.6.0)	Liao et al.[100]	https://subread.sourceforge.net/featureCounts.html
RSEM (version 1.3.1)	Li et al.[101]	https://github.com/deweylab/RSEM
edgeR (version 3.28.0)	Robinson et al.[102]	https://bioconductor.org/packages/release/bioc/html/edgeR.html
SNPsplit (version 0.3.4)	Krueger et al.[103]	https://github.com/FelixKrueger/SNPsplit
MACS2 (version 2.1.2)	Zhang et al.[104]	https://github.com/macs3-project/MACS
BEDtools (version 2.26.0)	Quinlan et al.[99,105]	https://bedtools.readthedocs.io/en/latest/
HOMER (version 5.0.1)	Heinz et al.[106]	http://homer.ucsd.edu/homer/download.html
Metascape	Zhou et al.[107]	https://metascape.org/gp/index.html#/ma in/step1
Sratoolkit (version 2.11.0)	N/A	https://github.com/ncbi/sra-tools
GraphPad Prism (version 8)	GraphPad Software	https://www.graphpad.com/features

EXPERIMANTAL MODEL AND STUDY PARTICIPANT DETAILS

Mice

Animal care

All animal experiments were performed in accordance with guidelines of the Institutional Animal Care and Use Committee at the RIKEN Center for Integrative Medical Sciences and RIKEN Bioresource Center. Same-sex littermates were housed in groups of up to five mice per ventilated cage with nesting materials. The mouse facility was kept at 21–25 °C and 40–60% humidity with a 12-h light and dark cycle. The age, strain, and sex of mice used in this study were 2-month-old B6D2F1 (BDF1) females (Jackson Laboratory), 3-6-month-old BDF1 males, and 3-6-month-old JF1/Msf males (RIKEN Bioresource Research Center, RBRC00639)[108]

METHOD DETAILS

Generation of oocyte-specific *Pcgf1/6/Mll2* conditional triple KO mice

Double LoxP sites were inserted into flanking regions of exon2 of *Mll2* in the $Zp3^{Cre}/Pcgf1^{fl/fl}/Pcgf6^{fl/fl}$ line[18] by using CRISPR/Cas9. Exon2 was targeted because its removal was known to result in early termination of translation and complete loss of function of MLL2.[109] Briefly, sgRNAs were designed at flanking regions of *Mll2* exon2 of by using the CRISPOR program[110] and generated with a GeneArt Precision gRNA Synthesis Kit (Thermo Fisher) according to the manufacturer's instructions. Cas9 mRNA (15 ng/μL), two sgRNAs (7.5 ng/μL each), and a template plasmid harboring the flox cassette and 1-2 kb homologous arms (25 ng/μL) were co-injected into both blastomeres of 2-cell embryos by using a Piezo impact-driven micromanipulator (Eppendorf).[111] The recipient 2-cell embryos had been generated by *in vitro* fertilization of sperm from $Zp3^{Cre}/Pcgf1^{fl/fl}/Pcgf6^{fl/fl}$ and oocytes from $Pcgf1^{fl/fl}/Pcgf6^{fl/fl}$ females. The mouse background was a B6.129 mixture. After obtaining a founder male that possessed the KI allele, it was mated with $Pcgf1^{fl/fl}/Pcgf6^{fl/fl}$ females to obtain $Zp3^{Cre}/Pcgf1^{fl/fl}/Pcgf6^{fl/fl}/Mll2^{flox/flox}$ males and $Pcgf1^{fl/fl}/Pcgf6^{fl/fl}/Mll2^{flox/flox}$ females. They were

Please cite this article in press as: Mei et al., H2AK119ub1-MLL2 counteraction underlies heritable H3K27me3 formation in oocytes, Molecular Cell (2026), https://doi.org/10.1016/j.molcel.2026.03.014

intercrossed to obtain *Zp3*^{Cre}/*Pcgf1*$^{fl/fl}$/*Pcgf6*$^{fl/fl}$/*Mll2*$^{flox/flox}$ (TKO) and *Pcgf1*$^{fl/fl}$/*Pcgf6*$^{fl/fl}$/*Mll2*$^{flox/flox}$ (WT) females for experiments. The primer and sgRNA sequences are listed in Table S5.

Generation of oocyte-specific *Pcgf1/6/C2MC* conditional triple KO mice

The C2MC, encoded in an intron of *Sfmbt2*, was deleted in the *Zp3*^{Cre}/*Pcgf1*$^{fl/fl}$/*Pcgf6*$^{fl/fl}$ line by using CRISPR/Cas9. Briefly, sgRNAs targeting the flanking regions of C2MC were designed in a previous study.[58] Recipient 2-cell embryos had been generated by *in vitro* fertilization of sperm from *Zp3*^{Cre}/*Pcgf1*$^{fl/fl}$/*Pcgf6*$^{fl/fl}$ and oocytes from *Pcgf1*$^{fl/fl}$/*Pcgf6*$^{fl/fl}$ females. Cas9 mRNA (30 ng/μL) and two sgRNAs (15 ng/μL each) were co-injected into a blastomere of the 2-cell embryos by using a Piezo impact- driven micromanipulator (Eppendorf). After obtaining founder females that possessed the KO allele, they were mated with *Zp3*^{Cre}/*Pcgf1*$^{fl/fl}$/*Pcgf6*$^{fl/fl}$ males to obtain *Zp3*^{Cre}/*Pcgf1*$^{fl/fl}$/*Pcgf6*$^{fl/fl}$/*C2MC*$^{+/-}$ females for experiments. The primer and sgRNA sequences are listed in Table S5.

Generation of oocyte-specific PRC1 catalytic dead (PRC1-CD) mice

The *Ring1a*-null mouse line has been previously reported.[93] The *Ring1b* I53A/D56K conditional point mutant (CPM) (*Ring1b*^{CPM}) mouse line was generated from M1 ESCs by using a previously developed KI cassette.[30] The M1 ESCs originated from an embryo derived from a C57BL/6JJcl and 129^{+Ter}/SvJcl cross. The *Ring1b* allele contains an I53A/D56K version of the exon encoding the E2 interaction domain in the antisense orientation downstream of the corresponding wild-type exon. This wild-type/mutant exon pair was flanked by inverted double LoxP sites. In the presence and absence of Cre expression, RING1B^{CPM} and wild-type RING1B are expressed, respectively.[30] The *Ring1a*-null and *Ring1b*^{CPM} females were crossed with a *Zp3*^{Cre} mouse line [Jackson Laboratory, C57BL/6-Tg(Zp3-cre)93Knw/J, 003651][43] to obtain *Zp3*^{Cre}/*Ring1a*$^{-/-}$/*Ring1b*$^{CPM/CPM}$ males and *Ring1a*$^{-/-}$/*Ring1b*$^{CPM/CPM}$ females. They were intercrossed to obtain *Ring1a*$^{-/-}$/*Ring1b*$^{CPM/CPM}$ (PRC1-WT) and *Zp3*^{Cre}/*Ring1a*$^{-/-}$/*Ring1b*$^{CPM/CPM}$ (PRC1-CD) females for experiments. The tail tips were used for genotyping. The PCR primer sequences are listed in Table S5.

Collection and culture of mouse oocytes and preimplantation embryos

FGOs were obtained from ovaries of 4-week-old females that had been injected with 0.12 mL of CARD HyperOva (Kyudo Co., Ltd) 46-48 hrs before collection. The ovaries were transferred to HEPES-buffered KSOM and the ovarian follicles were punctured with a 27-gauge needle. Cumulus cells were gently removed from cumulus-oocyte complexes (COCs) using a narrow-bore glass capillary. FGOs were transferred to Human Tubal Fluid (HTF) medium containing 0.2 mM 3-Isobutyl-1-methylxanthine (IBMX, Merck, I7018). Surrounded nucleolus (SN)-type FGOs were selected based on the presence of perivitelline spaces that appear only in SN-type oocytes after 1 hr of incubation in an IBMX-containing medium.[112] Only SN-type FGOs were used for experiments.

For *in vitro* fertilization of PRC1-WT and -CD oocytes, MII-stage oocytes were obtained from oviducts of 4- or 8-12-week-old superovulated females that had been injected with 5-7.5 IU PMSG followed by 5-7.5 IU human chorionic gonadotropin (hCG) at 48 hr intervals. MII oocytes were harvested 15–17 hrs after hCG injection and transferred to HTF supplemented with 10 mg/ml BSA (Merck Millipore; 12657). Spermatozoa were obtained from the caudal epididymis of adult B6D2F1 (BDF1) males (Jackson Laboratory) and capacitated by a 1 hr incubation in HTF. At 6–8 h post-insemination, fertilized oocytes with two pronuclei were transferred to KSOM and cultured under a humidified atmosphere with 5% CO2/95% air at 37.8 °C.

Chromatin transfer

Donor MII oocytes were collected from 4-week-old *Pcgf1*$^{fl/fl}$/*Pcgf6*$^{fl/fl}$/*Mll2*$^{flox/flox}$ (WT), *Zp3*^{Cre}/*Pcgf1*$^{fl/fl}$/*Pcgf6*$^{fl/fl}$ DKO), and *Zp3*^{Cre}/*Pcgf1*$^{fl/fl}$/*Pcgf6*$^{fl/fl}$/*Mll2*$^{flox/flox}$ (TKO) females that had been superovulated with 0.12 mL of CARD HyperOva (Kyudo Co., Ltd) followed by 5 IU hCG at 48 hr intervals. Recipient MII oocytes were collected from 8-week-old BDF1 females that had been superovulated with 7.5 IU PMSG followed by 7.5 IU hCG at 48 hr intervals. Cumulus cells were removed by a short incubation in M2 medium containing hyaluronidase (Millipore), and denuded oocytes were transferred to α-MEM (Thermo Fisher, 12571-063) supplemented with 5% FBS and 10 ng/ml EGF. Oocytes were transferred into M2 media containing 5 μg/ml cytochalasin B (Sigma-Aldrich). Zona pellucidae were cut by a Piezo impact- driven micromanipulator (Eppendorf) and the spindles were isolated from the oocytes. The Sendai virus (HVJ, Cosmo-bio) was used for fusing the spindles with recipient enucleated oocytes. Reconstructed oocytes were incubated in α-MEM/FBS/EGF for >1 hr until the fusion was complete. They were inseminated with sperm of BDF1 for embryo transplantation experiments or JF1/Msf (RIKEN Bioresource Research Center, RBRC00639)[108] for allelic RNA-seq experiments. Sperm capacitation was conducted by 1 hr incubation in HTF for BDF1 or 30 min incubation in CARD FERTIUP (Kyudo Co., Ltd) for JF1. At 6 hrs post-insemination, fertilized oocytes with two pronuclei were transferred to KSOM and cultured under a humidified atmosphere with 5% CO2/95% air at 37.8 °C.

Embryo transplantation, Caesarian section, and placental histology

After the reconstructed embryos reached the 2-cell stage, WT, *Pcgf1/6* matDKO, and *Pcgf1/6/Mll2* matTKO embryos were mixed and transferred into seven surrogate ICR strain mothers in two independent experiments. The numbers of embryos transplanted were 3-4 WT, 5 matDKO, and 5-6 matTKO per surrogate mother. The day of transplantation was counted as E0.5, and C-section was performed at E18.5. After counting the numbers of implantation sites and fetuses (5-11 fetuses per litter were recovered), measuring the weights of fetuses and placentae, and harvesting a small piece of the tails for genotyping *Pcgf1*-, *Pcgf6*-, and *Mll2*-KO alleles, the placentae were fixed in 4% paraformaldehyde (PFA) at 4°C overnight. The placental samples were then routinely

Please cite this article in press as: Mei et al., H2AK119ub1-MLL2 counteraction underlies heritable H3K27me3 formation in oocytes, Molecular Cell (2026), https://doi.org/10.1016/j.molcel.2026.03.014

embedded in paraffin. Serial sections (5 μm thickness) were subjected to H&E and periodic acid Schiff (PAS) staining. The genotyping primer sequences are listed in Table S5.

For the *Pcgf1/6*/C2MC matTKO experiment, MII-stage oocytes were obtained from *Pcgf1*$^{fl/fl}$/*Pcgf6*$^{fl/fl}$/*C2MC*$^{+/-}$ (producing the WT control) and *Zp3*^{Cre}/*Pcgf1*$^{fl/fl}$/*Pcgf6*$^{fl/fl}$/*C2MC*$^{+/-}$ females (producing the *Pcgf1/6* matDKO and *Pcgf1/6*/ C2MC matTKO groups). The oocytes were fertilized with BDF1 sperm and transplanted into 13 surrogate ICR strain mothers in two independent experiments. The numbers of embryos transplanted were 4 WT and 20 matDKO/matTKO mixture per surrogate mother. Consequently, 4-12 fetuses per litter were recovered. Genotyping was performed for *Pcgf1*-, *Pcgf6*-, and C2MC-KO alleles. The primer sequences are listed in Table S5.

Whole mount immunostaining

FGOs were fixed with 3.7% PFA containing 0.2% Triton X-100 at room temperature (RT) for 20 min. After washing 3 times with PBS containing 1% BSA (PBS/BSA), the oocytes were treated with mouse anti- H3K27me3 (1/500, Active Motif, #61017, MABI0323), anti-H3K4me3 (1/500, Millipore 05-1339), and rabbit anti-H2AK119ub1 (1/2,000, Cell Signaling Technology, #8240) antibodies at 4°C overnight. The specificities of these antibodies were proven in previous studies[18] and this study. After washing with PBS/BSA, they were incubated with a 1:250 dilution of Alexa Flour 488 donkey anti-mouse IgG and Alexa Flour 568 donkey anti-rabbit IgG (Life Technologies) in PBS/BSA at RT for 1 h. The samples were washed 3 times and then mounted on a glass slide in Vectashield anti-fade solution with 4',6-diamidino-2- phenylindole (DAPI) (Vector Laboratories, Burlingame, CA). Fluorescence was detected under a confocal microscope, Leica TCS Sp8. All images were acquired and quantified using LASX software (Leica). Briefly, the nuclear signal intensity of oocytes was determined and the cytoplasmic signal was subtracted as background. After the signal values were divided by the DAPI signal intensity in each oocyte, the average signal intensity of control oocytes was set as 1.0.

Carrier Assisted ChIP-seq (CATCH-seq)

CATCH-seq is an improved method of the ultra-low-input native ChIP-seq (ULI-NChIP).[113] The original protocol of CATCH-seq was described in Zhu et al.[45] and we have made some modifications to improve its usability.[33] After ZP were removed by acid Tyrodes' solution, ZP-free SN oocytes were washed in 0.2%BSA/PBS and collected in 9 μL of Nuclei EZ lysis buffer (Sigma, NUC-101) supplemented with a complete EDTA- free protease inhibitor cocktail and 1 mM phenylmethanesulfonyl fluoride. The samples were snap-frozen in liquid nitrogen and stored at -80°C until use. On the day of library construction, the samples were thawed on ice and 1 μL of the lysis buffer containing a constant number of Drosophila melanogaster S2 cells was added (Thermo Fisher Scientific, R69007) for spike-in normalization purposes. Then, 1 μL of a 1% Triton X-100 (Merck 93443) and 1% deoxycholate (Nacalai, 10712-54) mixture solution was added to the samples, which then sat on ice for 5 min. The chromatin was fragmented using 2 U/μl MNase (M0247S, NEB) in 1xMNase buffer supplemented with 1% PEG6000 (Hampton Research, HR2-533) and 2 mM DTT (Nacalai) at 21°C for 7.5 min. The MNase reaction was stopped by adding 1/10 volume of 100 mM EDTA and 1/12 volume of the 1% Triton X-100 and 1% deoxycholate mixture, then the samples were rested on ice for 15 min. The chromatin lysates were then added with freshly prepared immunoprecipitation buffer,[113] and 5% volume was kept for input library construction. To the rest of the lysate, 30 ng of annealed I-SceI carrier DNA was added.[45] The forward and reverse strands of the carrier DNA were as follows: /5AmMC6/Gtagggataacagggtaattagggataacagggtaattagggataacagggtaattagggataacagggtaattagggataacagggtaattagggataacagggtaat*c/3AmMO/ and /5AmMC6/Gattaccctgttatccctaattaccctgttatccctaattaccctgttatccctaattaccctgttatccctaattaccctgttatccctaattaccctgttatcccta*c/3AmMO/, respectively, where asterisks represent phosphorothioate bonds. The oligos were synthesized by Integrated DNA Technologies. For each immunoprecipitation reaction, 0.25 μL of rabbit anti-H3K4me3 (Active Motif 39159, 70 oocytes/library), 500 ng of rabbit anti-H3K27me3 (Diagenode C15410069, 50-80 oocytes/library), 1.0 μg of mouse anti-H3K36me2 (MBL, MABI0332, 100 oocytes/library) or 1.0 μL of rabbit anti-H3K36me3 antibody (Active Motif 61022, MABI0333, 100 oocytes/library) conjugated to a precleared Dynabeads Protein A (Thermo Fisher Scientific, 10006D) and G (Thermo Fisher Scientific, 10007D) mixture was used. The specificity of these antibodies was validated in previous studies [H3K4me3,[114] H3K27me3,[21] H3K36me2[52,54,55] and H3K36me3[52,54,56]]. After immunoprecipitation at 4°C overnight, the chromatin-Dynabeads were washed twice each with the low and high salt wash buffers, and the chromatin was eluted in the freshly prepared ChIP elution buffer at 65°C for 1 hr.[113] DNA was recovered by phenol-chloroform extraction followed by ethanol precipitation. Adaptor ligation was performed by NEBNext Ultra II DNA Library Prep Kit for Illumina (E7645, NEB) in a half scale of the manufacturer's instruction, and the libraries were purified by 1.8x SPRIselect beads (B23318, Beckman Coulter). The DNA was amplified by KAPA Hifi 2X mater PCR mix (KK2605) for 13-15 PCR cycles with dual indexing primers (NEBNext Multiplex Oligos for Illumina, E6440). After purification with 0.9x SPRIselect beads, the samples were digested by I-SceI (5 U/μl, NEB, R0694) at 37°C for 2 hrs followed by heat inactivation at 65°C for 20 min and purified by 0.9x SPRIselect beads. The second amplification was not performed. The libraries were sequenced on Nextseq500 or Nextseq2000 with paired- end or single-end reads (Illumina).

CUT&RUN

CUT&RUN libraries were prepared as previously described.[115] The antibodies used were rabbit anti-H3K27me3 (1/100, Diagenode C15410069, 150-170 oocytes/library) and anti-H2AK119ub1 (1/50,CST8240, 300 oocytes/library). Protein A-MNase was provided by Dr. Steven Henikoff's laboratory.[116] CUT&RUN libraries were sequenced on a NextSeq500 or Nextseq2000 with paired-end or single-end reads (Illumina)

Please cite this article in press as: Mei et al., H2AK119ub1-MLL2 counteraction underlies heritable H3K27me3 formation in oocytes, Molecular Cell (2026), https://doi.org/10.1016/j.molcel.2026.03.014

RNA-seq

FGOs and F1 hybrid embryos were prepared as described above. For bulk RNA-seq of PRC1-WT and - CD FGOs, ten oocytes were pooled to generate each RNA-seq library. Zona pellucida were removed by brief incubation in Acidic Tyrode's solution. The samples were washed three times in 0.2% BSA/PBS before being transferred into a 0.2 ml tube with ~0.5 μl carryover. RNA-seq libraries were prepared as previously described.[33] Briefly, cDNA was prepared by SMART-Seq v4 Ultra Low Input RNA Kit for Sequencing (TAKARA, 634890) according to the manufacturer's instructions. Two hundred picograms of cDNA were used for the library construction by using Nextera XT DNA Library Preparation Kit (Illumina, FC-131-1024) according to the manufacturer's instructions. All RNA-seq libraries were sequenced on a NextSeq500 with single-end 75 bp reads (Illumina).

QUANTIFICATION AND STATISTICAL ANALYSIS

Low-input chromatin profiling data analyses

The sequencing read information in this study is found in Table S6. Low-quality bases and adapters in the sequencing reads of CATCH-seq, CUT&RUN, ChIP-seq and ATAC-seq were trimmed by TrimGalore (https://github.com/FelixKrueger/TrimGalore) (version 0.6.4). Then, all clean reads were mapped to the mouse reference genome (mm10) using Bowtie2[94] (version 2.3.5) with the parameters ''-q -N 1 -L 25''. After removing PCR duplicates by Sambamba[95] with the parameters 'markdup -r -t 2' and filtering out multiple mapping reads, uniquely mapped reads were used for the downstream analysis. Samtools[96] (version 1.7) was used to manipulate the SAM and BAM files. For the visualization using the Integrative Genomics Viewer[97] (version 2.8.0), genome-wide coverage tracks were generated using the 'bamCoverage' function from the deepTools[98] suite with the parameters '–binSize 50 –normalizeUsing RPKM'. To compare replicates, read counts over 5-kb bins across the whole genome were calculated and the RPM (reads per million) values were used to calculate the correlation coefficient. Biological replicates were merged for the visualization and other analyses after validating the reproducibility.

RNA-seq data analyses

All RNA-seq read after trimming by TrimGalore (version 0.6.4) (https://github.com/FelixKrueger/TrimGalore) were aligned to the mouse reference genome (mm10) by STAR[99] with default parameters '–runMode alignReads –outSAMattributes NH HI NM MD – outSAMtype BAM Unsorted'. Raw read counts for each gene were calculated by featureCounts[100] (version 1.6.0) with the parameters '-s 0 -t exon -g gene_id' based on the mm10 ncbiRefSeq annotation file from. Then, differentially expressed genes were identified by the edgeR[102] R package (version 3.28.0) under the 'glm' framework. The gene expression levels were calculated by RSEM[101] (version 1.3.1) to make the correlation analyses between biological replicates and downstream analysis.

For allele-specific analysis of BDF1 x JF1 hybrid embryos, the SNPs in BDF1 and JF1 were masked as 'N' in the reference genome (GRCm38) by the 'Dual strain mode' in SNPsplit_genome_preparation of SNPsplit[103] (version 0.3.4). Then reads were aligned to the N-masked genome by STAR[99] (version 2.7.6) with specific setting of parameters '–alignEndsType EndToEnd –outSAMattributes NH HI NM MD'. By filtering the alignment records with the 'NH:i:1' tag, uniquely aligned reads were assigned to its parental origins. SNPsplit[103] was used to assign the SNP-containing reads to maternal and paternal genomes. The number of allelic reads of each gene was calculated by featureCounts[100] (version 1.6.0) to calculate the RPKM values.

Identification of high-confidence H3K27me3-harboring genes

To define high-confidence H3K27me3-harboring genes, MACS2[104] (version 2.1.2) was used for peak calling with the parameters '-g mm –nomodel –nolambda –broad' for all H3K27me3 CATCH-seq and CUT&RUN in WT FGOs, including the public datasets of *Pcgf1/6* CTR FGOs (Mei et al.[18]). Then, their intersection was selected by BEDtools[105] (version 2.26.0) for further analysis. As for genes with multiple transcription start sites (TSSs), promoter regions (TSS ± 2 kp) overlapped with H3K27me3 peaks were selected to check whether H2AK119ub1 peaks were occupied. If the genes had at least a promoter with both H3K27me3 and H2AK119ub1 enrichment, they were considered to be high-confidence H3K27me3-harboring genes. For gene body analysis of genes encoding multiple transcripts, high- confidence H3K27me3-harbored genes were defined by those containing at least one transcript with both H3K27me3 and H2KA119ub1 peaks.

Comparison of histone modification at promoters and gene bodies in WT and mutants

All clean reads of spike-in CATCH-seq and CUT&RUN were aligned to the mouse and *D.melanogaster* genome sequences (mm10 + dm6) using Bowtie2[94] with default parameters. Only uniquely mapped reads were considered to be spike-in reads. Spike-in normalization was performed using the exogenous scaling factor, which was calculated by the formula (scaling factor = 1/(spike-in reads/1,000,000)). Then, the spike- in scaled signal tracks were generated by bamCoverage from deeptools[98] with the parameters '—scaleFactor scaling factor –binSize 50 –normalizeUsing RPKM'. A tool named 'computeMatrix' from the deepTools suite was used to calculate the average enrichment level of histone modifications. The fold changes of enrichment level between in WT and mutants were calculated to compare the differences and identify differentially modified promoters or gene bodies.

Please cite this article in press as: Mei et al., H2AK119ub1-MLL2 counteraction underlies heritable H3K27me3 formation in oocytes, Molecular Cell (2026), https://doi.org/10.1016/j.molcel.2026.03.014

Transcription factor motif enrichment and Gene ontology analysis

To identify transcription factor binding motifs at promoter, findMotifsGenome.pl from HOMER[106] program was used by selecting all promoter sequences as background. GO enrichment analysis was performed by Metascape.[107] Significantly representative Biological Process (BP) terms were selected to visualize (q-value < 0.01).

Chromatin states analysis and genomic annotation analysis

ChromHMM[41] (version 1.27) was used to classify chromatin states based on five histone modifications. All alignment files for each histone modification were binarized using the 'BinarizeBam' command with a bin size of 2 kb (option '-b 2000'). Then, genomic regions were classified into 10 ChromHMM types using the 'LearnModel' command with 2-kb bins. H3K36me2-gain bins were annotated by ChIPseeker[117] (version 1.22.1) with the priority order (promoter > exon > intron > downstream > intergenic) if one peak spanned multiple genomic features.

Analysis of publicly available data

All files in SRA format were downloaded and converted into fastq files by sratoolkit (https://github.com/ncbi/sra-tools) (version 2.11.0). Reads were pre-processed and subjected to the corresponding analyses as described above.

Molecular Cell, Volume *86*

Supplemental information

H2AK119ub1-MLL2 counteraction underlies heritable H3K27me3 formation in oocytes

Hailiang Mei, Chisayo Kozuka, Mami Kumon, Haruhiko Koseki, and Azusa Inoue

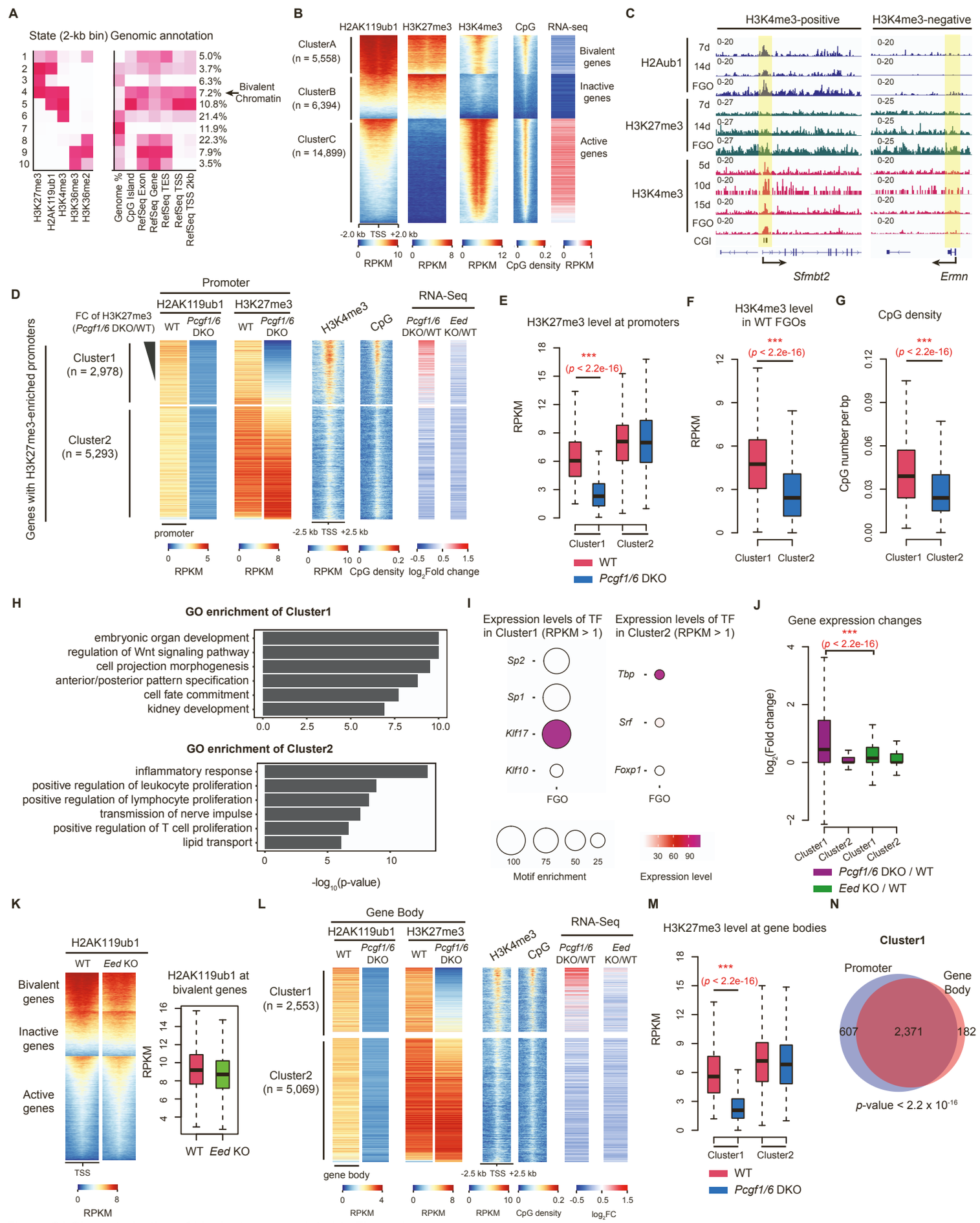

Figure S1 Characterization of bivalent genes, related to Figure 1.

A, Heatmap illustrating different chromatin states defined by five indicated histone modifications using ChromHMM.

B, Heatmaps showing three histone modifications levels, CpG density, and gene expression levels at promoters of three clusters (K-means = 3) in WT FGO.

C, Genome browser views of the indicated histone modifications during oocyte growth at H3K4me3-positive and H3K4me3-negative genes. Promoter regions are highlighted in yellow.

D, Heatmaps showing the levels of H2AK119ub1 and H3K27me3 at promoters of all high-confidence H3K27me3 harboring genes in WT and *Pcgf1/6* DKO FGOs. Two clusters were defined by the fold change of H3K27me3 (WT/DKO) over or less than 1.5, respectively. H3K4me3 and CpG-density heatmaps indicate the signal enrichment around TSSs in WT FGOs. The RNA-seq column indicates the fold change of gene expression.

E, F, G, Box plots showing the H3K27me3 levels (**E**), H3K4me3 levels (**F**), and CpG density (**G**) at TSS +/-2.5 kb region of genes in Cluster1 and Cluster2. The p-value was calculated by a two-sided Mann-Whitney *U*-test.

H, Gene ontology terms enriched in Cluster1 and 2, respectively. **I**, Bubble plots showing the expression levels of TFs (RPKM > 1) and the statistical significance of motif enrichment (P-value of hypergeometric test with one-sided) in Cluster1 and 2, respectively.

J, Box plots showing the fold change of gene expression levels between *Pcgf1/6* WT and DKO and between *Eed* WT and KO FGOs.

K, Heatmaps showing signal enrichment of H2AK119ub1 in WT and *Eed* KO FGOs. The box plot indicates the levels of H2AK119ub1 at bivalent promoters.

L, Heatmaps showing the average levels of H2AK119ub1 and H3K27me3 across gene bodies of high-confidence H3K27me3-harboring genes. Each row represents average levels of the indicated histone modifications within each gene body. Two clusters were defined by the fold change of H3K27me3 (WT/DKO) over or less than 1.5, respectively. The H3K4me3 and CpG-density heatmaps indicate the signal enrichment around TSSs in WT FGOs. RNA-seq columns indicate the relative gene expression in FGOs [log2 FC (KO/WT)].

M, Box plots showing the average signals of H3K27me3 across gene bodies in *Pcgf1/6* DKO and WT FGOs.

N, Venn diagrams showing the overlap between genes losing promoter H3K27me3 and those losing gene body H3K27me3. The p-value was calculated by a two-sided Fisher's exact test.

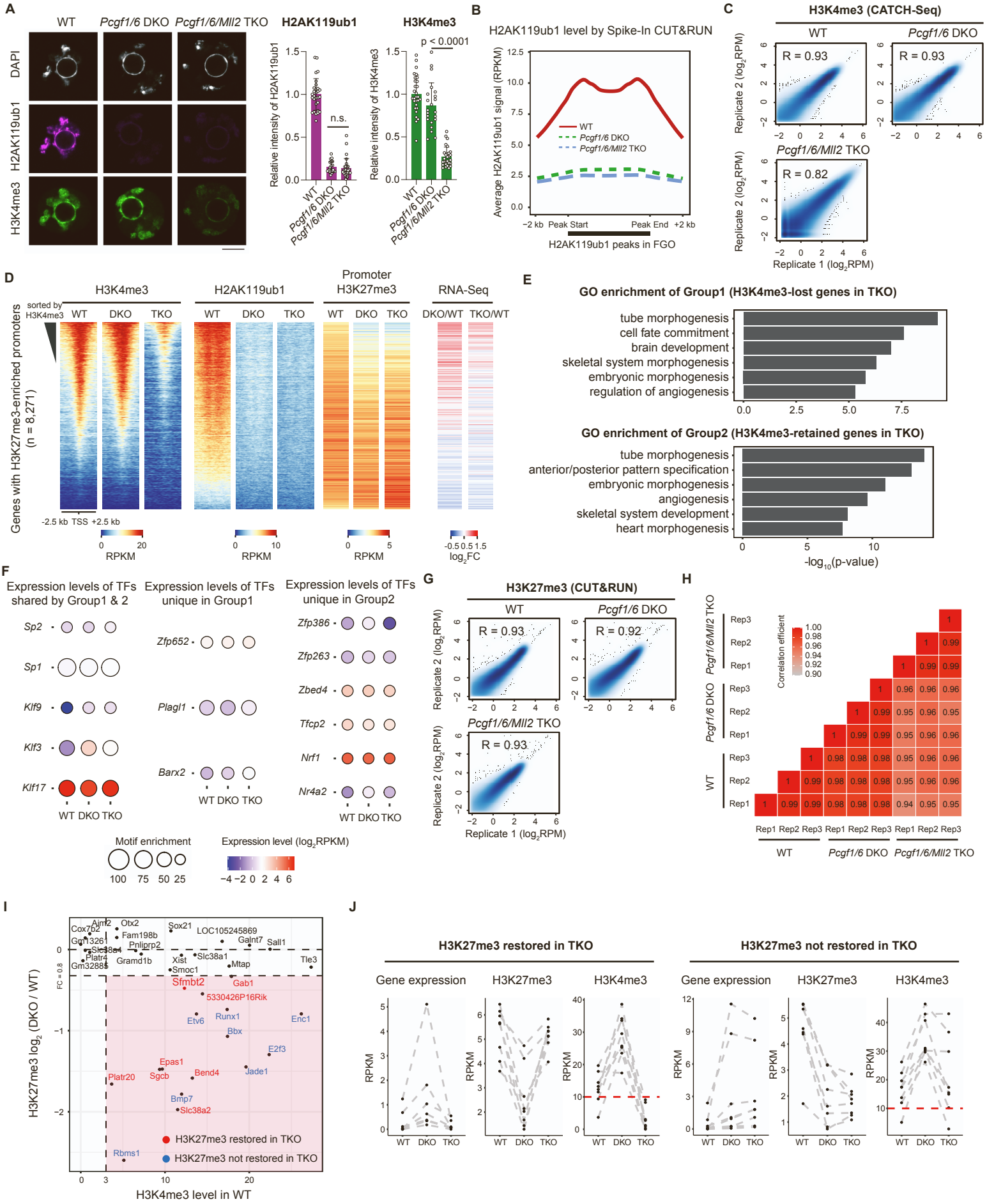

Figure S2 Characterization of *Pcgf1/6/Mll2* TKO fully grown oocytes (FGOs), related to Figure 2.

A, Representative images (left) and quantification (right) of FGOs immunostained with anti-H2AK119ub1 and H3K4me3 antibodies. The average signal intensity of WT oocytes was set as 1.0. The total number of oocytes examined in three independent experiments are 29 (WT), 22 (DKO), and 29 (TKO). p, two-tailed Student's t-test.

B, Average signal profiles of H2AK119ub1 spike-in CUT&RUN at peak regions in WT, *Pcgf1/6* DKO, and *Pcgf1/6/Mll2* TKO FGOs.

C, Scatter plots showing the correlations between biological replicates of H3K4me3 CATCH-seq in FGOs.

D, Heatmaps showing the signal intensities of the indicated histone modifications at promoters of H3K27me3-enriched genes in WT, *Pcgf1/6* DKO, and *Pcgf1/6/Mll2* TKO FGOs. The row was sorted by basal H3K4me3 level of WT FGOs in descending order. RNA-seq columns indicate the relative gene expression in FGOs (log2FC).

E, Gene ontology terms enriched in Cluster1 and 2, respectively.

F, Bubble plots showing the expression level of TFs unique in Group1 (left) and 2 (right), respectively, and the statistical significance of the motif enrichment (P-value of hypergeometric test with one-sided).

G, Scatter plots showing the correlations between biological replicates of H3K27me3 CUT&RUN in FGOs.

H, Correlations between biological replicates of RNA-seq in FGOs.

I, Scatter plot showing the levels of promoter H3K4me3 in WT FGOs and the extent of H3K27me3 loss in *Pcgf1/6* DKO at noncanonical imprinted genes. Genes harboring promoter H3K4me3 (RPKM>3 in WT) and losing H3K27me3 [FC(DKO/WT)<0.8] are highlighted by a pink box.

J, Line plots showing the levels of gene expression, H3K27me3, and H3K4me3 in genes restoring or not restoring H3K27me3 in TKO FGOs, respectively.

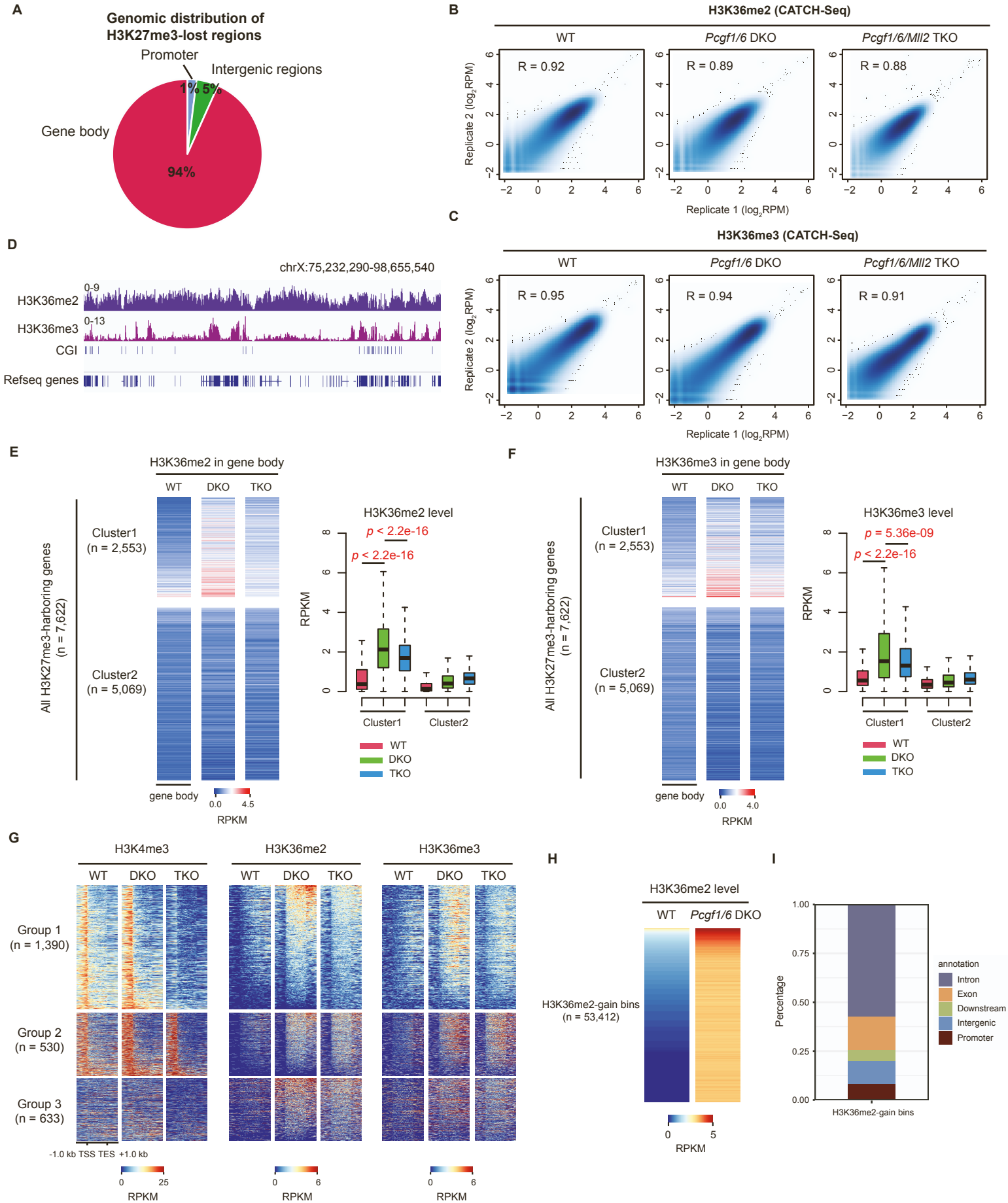

Figure S3 Characterization of H3K36me2 and H3K36me3 in *Pcgf1/6* DKO and *Pcgf1/6/Mll2* TKO FGOs, related to Figure 3.

A, A pie chart showing the proportion of H3K27me3-lost regions in *Pcgf1/6* DKO FGOs.
B, C, Scatter plots showing the correlations between biological replicates of H3K36me2 (**B**) and H3K36me3 (**C**) CATCH-seq in FGOs.
D, A genome browser view of differential distribution of H3K36me2 and 3 across the X chromosome in WT FGOs.
E, **F**, Heatmaps and boxplots showing the average levels of H3K36me2 (**E**) and H3K36me3 (**F**) in gene bodies of all high-confidence H3K27me3-harboring genes. The p-values were calculated by a Mann-Whitney U-test.
G, Heatmaps showing the signal enrichment of three modifications from TSS to TES.
H, Heatmaps showing H3K36me2 level of all H3K36me2-gain bins.
I, Genomic annotation of the H3K36me2-gain bins.

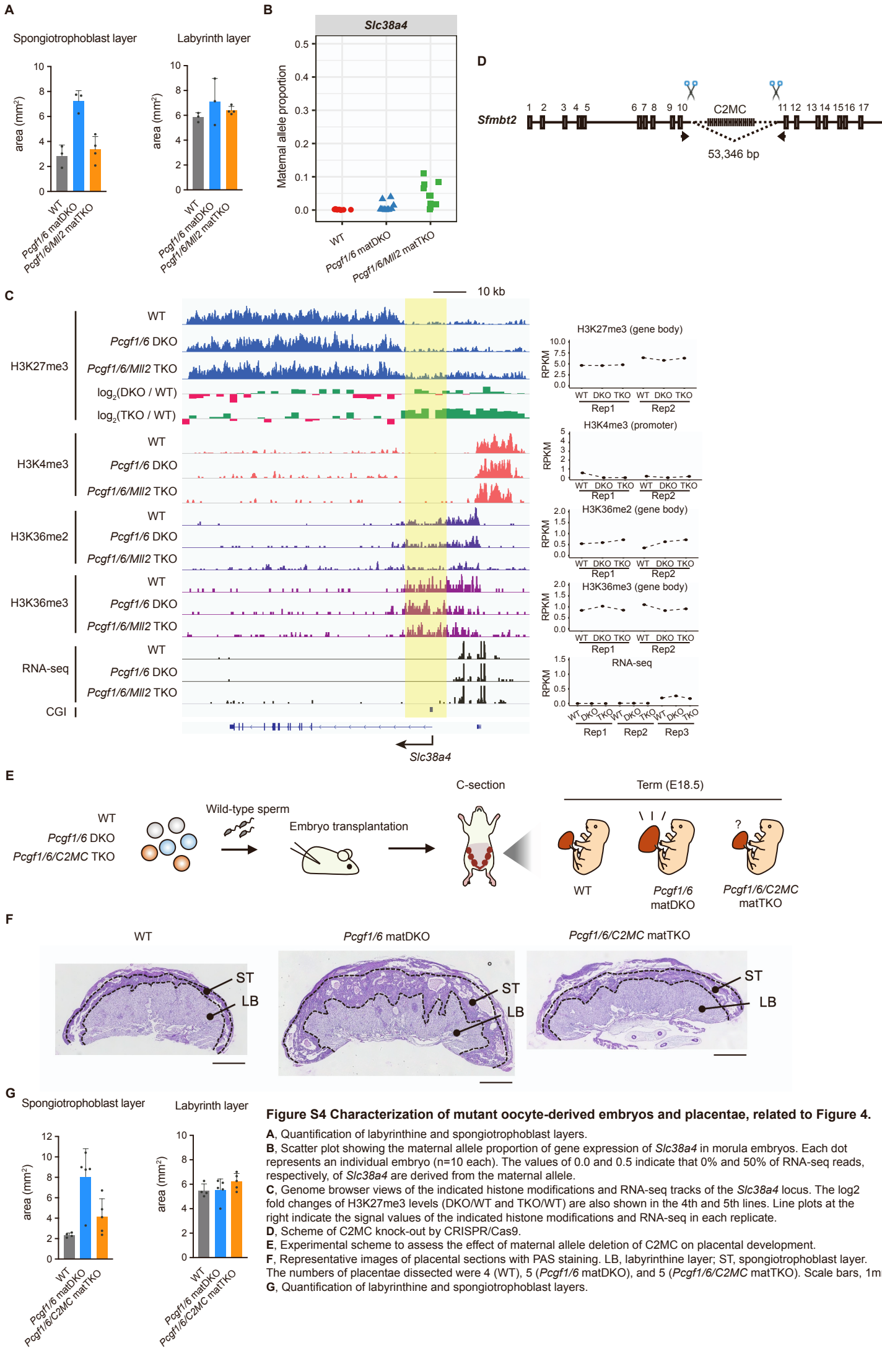

Figure S4 Characterization of mutant oocyte-derived embryos and placentae, related to Figure 4.

A, Quantification of labyrinthine and spongiotrophoblast layers.
B, Scatter plot showing the maternal allele proportion of gene expression of *Slc38a4* in morula embryos. Each dot represents an individual embryo (n=10 each). The values of 0.0 and 0.5 indicate that 0% and 50% of RNA-seq reads, respectively, of *Slc38a4* are derived from the maternal allele.
C, Genome browser views of the indicated histone modifications and RNA-seq tracks of the *Slc38a4* locus. The log2 fold changes of H3K27me3 levels (DKO/WT and TKO/WT) are also shown in the 4th and 5th lines. Line plots at the right indicate the signal values of the indicated histone modifications and RNA-seq in each replicate.
D, Scheme of C2MC knock-out by CRISPR/Cas9.
E, Experimental scheme to assess the effect of maternal allele deletion of C2MC on placental development.
F, Representative images of placental sections with PAS staining. LB, labyrinthine layer; ST, spongiotrophoblast layer. The numbers of placentae dissected were 4 (WT), 5 (*Pcgf1/6* matDKO), and 5 (*Pcgf1/6/C2MC* matTKO). Scale bars, 1mm.
G, Quantification of labyrinthine and spongiotrophoblast layers.

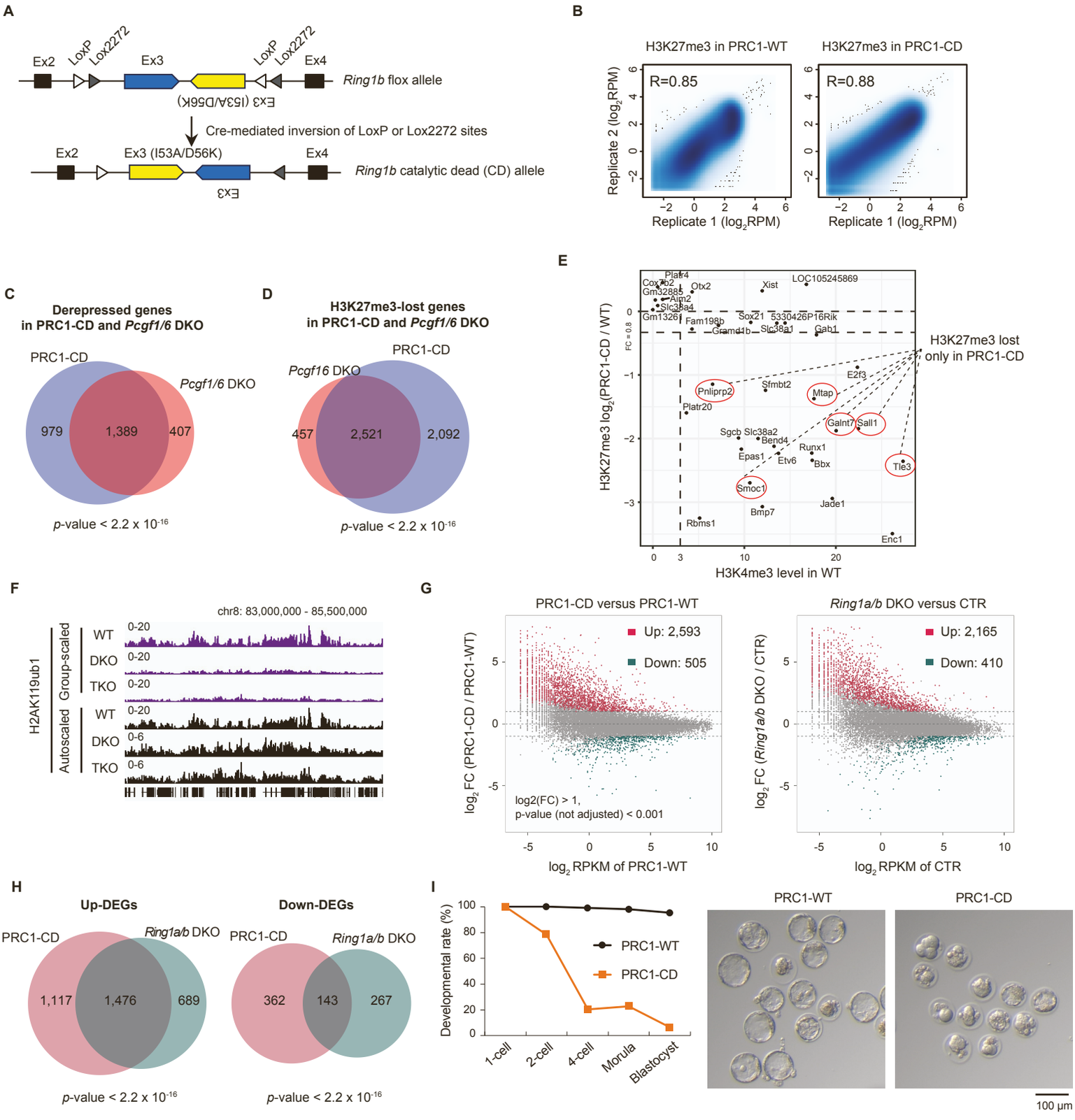

Figure S5 Characterization of PRC1-catalytic dead (CD) FGOs, related to Figure 5.

A, Scheme of generation of conditional *Ring1b* catalytic dead model.
B, Scatter plots showing the correlation between biological replicates of H3K27me3 CATCH-seq in PRC1-WT and PRC1-CD FGOs.
C, **D**, Venn diagrams showing the overlap of derepressed genes (**C**) and H3K27me3-lost genes (**D**) between PRC1-CD and *Pcgf1/6* DKO FGOs. The p-value ($p < 2.2e-16$) was calculated by a two-sided Fisher's exact test.
E, Scatter plot showing the levels of promoter H3K4me3 in WT FGOs and the extent of H3K27me3 loss in PRC1-CD FGOs at noncanonical imprinted genes. Genes losing H3K27me3 only in PRC1-CD FGOs, but not *Pcgf1/6* DKO FGOs, are highlighted by red circles.
F, Genome browser views of H2AK119ub1. Note that residual H2AK119ub1 in DKO and TKO FGOs is detected at regions originally enriched in WT FGOs, which becomes apparent when IGV tracks are visualized using autoscale.
G, MA plots showing the fold change of gene expression levels in PRC1-CD and *Ring1a/b* DKO FGOs. Significantly up- and down-regulated genes (FC > 2, p-value < 0.001) are highlighted. The RNA-seq datasets of *Ring1a/b* DKO FGOs are from Du et al. (GSE132156).
H, Venn diagrams showing the overlap of up-regulated differentially expressed genes (Up-DEGs) and down-regulated DEGs in PRC1-CD and *Ring1a/b* DKO FGOs. DEGs are defined by p-value < 0.001 (not adjusted) and $|FC| > 2$.
I, Percentage of embryos that reached the indicated stage of preimplantation development (left) and representative images of embryos at 96 hours post-insemination (right). The number of embryos examined in 3 independent experiments was 105 (PRC1-WT) and 79 (PRC1-CD).

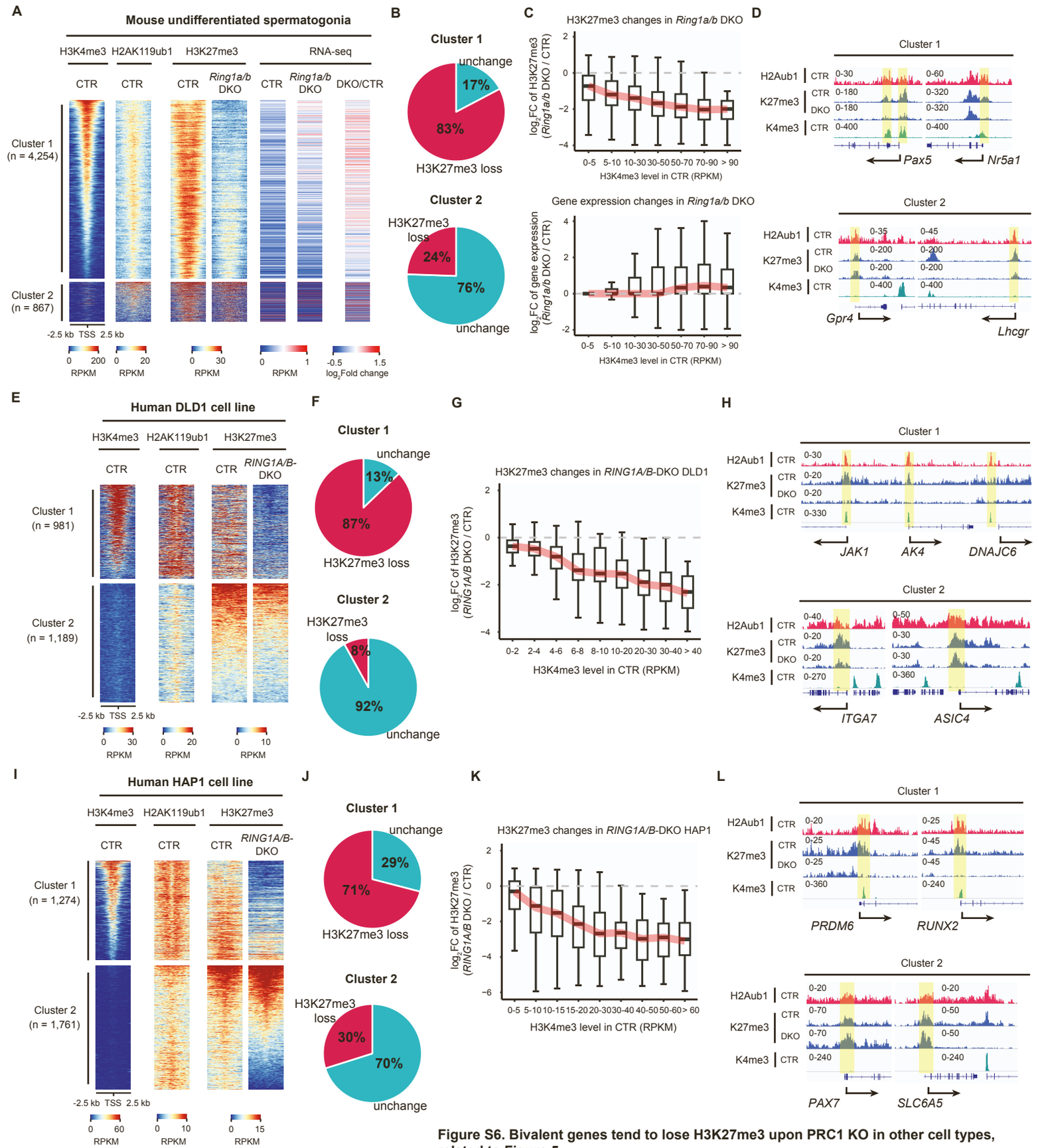

Figure S6. Bivalent genes tend to lose H3K27me3 upon PRC1 KO in other cell types, related to Figure 5.

A, Heatmaps showing the signal intensities of the indicated histone modifications at promoters of H3K27me3-harboring genes in mouse undifferentiated spermatogonia. Two clusters of H3K27me3-enriched genes at promoter are defined by the presence or absence of H3K4me3 peaks. The H2AK119ub1, H3K27me3, H3K4me3 CUT&Tag and RNA-seq datasets are from Hu et al. (GSE221942).

B, Pie chart showing the proportion of H3K27me3-lost genes in the two clusters.

C, Box plots showing the fold changes of promoter H3K27me3 and gene expression levels between CTR and *Ring1a/b* DKO spermatogonia. The red lines in the boxes represent median values.

D, Genome browser views in control (CTR) and *Ring1a/b* DKO spermatogonia. Promoter regions are highlighted in yellow.

E, Heatmaps showing the signal intensities of the indicated histone modifications at promoters of H3K27me3-harboring genes in the human DLD1 cell line. Two clusters are defined as described in panel a. The H2AK119ub1 and H3K27me3 ChIP-seq datasets are from Sijm et al. (GSE193014). The H3K4me3 ChIP-seq datasets are from Wan et al. (GSE156081).

F, Pie chart showing the proportion of H3K27me3-lost genes in the two clusters.

G, Box plots showing the fold changes of promoter H3K27me3 between CTR and *RING1A/B* DKO DLD1 cell line. The red lines in the boxes represent median values.

H, Genome browser views in CTR and *RING1A/B* DKO DLD1 cells.

I, Heatmaps showing the signal intensities of the indicated histone modifications at promoters of H3K27me3-harboring genes in the human HAP1 cell line. Two clusters are defined as described in panel a. The H2AK119ub1 and H3K27me3 ChIP-seq datasets are from Sijm et al. (GSE193013). The H3K4me3 ChIP-seq datasets are from Peeters et al. (GSE107599).

J, Pie chart showing the proportion of H3K27me3-lost genes at promoters in the two clusters.

K, Box plots showing the fold changes of promoter H3K27me3 between CTR and *RING1A/B* DKO HAP1 cell line. The red lines in the boxes represent median values.

L, Genome browser views in CTR and *RING1A/B* DKO HAP1 cells.

M, Genome browser view of H3K4me3 distribution at the *Sfmbt2* locus in *Pcgf1/6* maternal DKO blastocyst embryos.